Flow and Wake Length Downstream of Live Submerged Vegetation Patches: How Do Different Species and Patch Configurations Create Sheltering in Stressful Habitats?

Loreta Cornacchia, Nicolas Riviere, J. John Soundar Jerome, Delphine Doppler, Félix Vallier, Sara Puijalon

Flow and wake length downstream of live submerged vegetation patches: how do different species and patch configurations create sheltering in stressful habitats?

Loreta Cornacchia[1]*, Nicolas Riviere[2], J. John Soundar Jerome[2], Delphine Doppler[2], Félix Vallier[1], Sara Puijalon[1]

[1] Univ Lyon, Université Claude Bernard Lyon 1, CNRS, ENTPE, UMR 5023 LEHNA, F-69622, 43 Boulevard du 11 Novembre 1918, F-69100, Villeurbanne, France.

[2] Univ Lyon, Université Claude Bernard Lyon I, Ecole Centrale de Lyon, INSA Lyon, CNRS, LMFA, UMR 5509, 43 Boulevard du 11 Novembre 1918, F-69100, Villeurbanne, France.

Corresponding author: Loreta Cornacchia (loreta.cornacchia@nioz.nl)

* Current address: NIOZ Royal Netherlands Institute for Sea Research, Department of Estuarine and Delta Systems, P.O. Box 140, 4400 AC Yerseke, The Netherlands

Key Points:

- Vegetation patches in stressful habitats shelter organisms from hydrodynamic forces.
- The sheltering effect is influenced by two fundamental patch dimensions (i.e., canopy half-width and height) and by patch density.
- Flow attenuation behind channel-spanning patches prevails for longer distances than for finite-width patches.

Abstract

Vegetated canopies modify water conveyance and bed stabilization in aquatic ecosystems, providing shelter for other organisms. The sheltering effect downstream of a canopy is however rarely quantified for live vegetation, and it is unknown how this effect is influenced by vegetation patch configuration and characteristics. We measured the sheltering effect of different species and patch configurations by comparing the length of the steady wake region, defined in this study as (1) the zone where streamwise velocity is diminished to more than half of the incoming velocity (L_{w1}), and (2) the distance downstream of the patch where velocity begins to increase (L_{w2}). Then, we measured the drag experienced by a plant at different downstream locations as a measure of sheltering for plants growing in the steady wake. We found that L_{w1} for channel-spanning cases was longer than for finite-width cases and extended to ≥ 2.5 patch lengths from the patch leading edge, while L_{w2} for finite-width patches was related to the smallest dimension between canopy half-width and height. Species effects were consistent across definitions: the species with the longest wake lengths was *G. densa*, followed by *C. platycarpa* and *V. spiralis*, which showed similar wake lengths for finite-width cases. Drag reduction was related to downstream flow modification for finite-width patches, but not for channel-spanning ones. The results of this study indicate that patterns of hydrodynamic sheltering behind live patches can be complex and difficult to predict based only on patch dimensions, especially due to co-variation between patch characteristics in real vegetation.

1 Introduction

Many ecosystems are modified by the actions or physical structure of organisms called ecosystem engineers (Jones et al., 1994). In aquatic environments, macrophytes act as important engineering species (Gurnell, 2014). They affect nutrient cycles and provide food and shelter for other organisms, such as fish and invertebrates (Haslam, 1978; Franklin et al., 2008). Vegetation promotes the deposition of finer, nutrient-rich sediment (Cotton et al., 2006; Wharton et al., 2006) and, at a larger scale, can affect geomorphic adjustments and landscape evolution (Gurnell & Grabowski, 2016). Vegetation also plays an important role by modifying hydrodynamic forces, water conveyance and bed stabilization (Sand-Jensen & Mebus, 1996; Sand-Jensen, 1998; Sukhodolov & Sukhodolova, 2009; Nepf, 2012).

In running water habitats, vegetation often grows in patches, which are relatively well-defined areas that differ from their surroundings (Forman, 1995). Patches generally consist of a single species at a relatively high density, and their spatial properties (e.g., length, width) are identified by sharp edges compared to surrounding bare areas (Schoelynck et al., 2018). Flow velocities are attenuated and sedimentation is enhanced within the patches (Bouma et al., 2007; Schoelynck et al., 2012; Licci et al., 2019); turbulence can either be reduced inside the patches and promote sediment deposition (Schulz et al., 2003; Hendriks et al., 2008), or it can increase at the plant stem scale, leading to resuspension of sediments (Tinoco & Coco, 2016). Flow velocity and turbulence are also reduced downstream of the canopy, leading to increased fine sediment deposition (Sand-Jensen, 1998). Although sediment deposition is enhanced behind the vegetation, scour patterns tend to form around the vegetation (Bouma et al., 2007; Chen et al., 2012a; Follett & Nepf, 2012; Yager & Schmeeckle, 2013) and partly contribute to the deposition behind vegetation patches. This flow velocity reduction creates a sheltered region downstream of the vegetation, which is considered a major process for the functioning of running water ecosystems (Cornacchia et al., 2018; Baladrón et al., 2021). In physically harsh environments, a reduction in environmental stress is important for the structure of natural communities (Bertness & Callaway, 1994; Bruno et al., 2003). Running water habitats produce highly challenging conditions (Denny, 1988; Vogel, 1994), with a continuous risk of mechanical failure, dislodgement and downstream transport. Therefore, vegetation patches represent a major shelter for several types of organisms. For example, macrophyte patches generate a protected environment allowing the development of dense invertebrate communities (Gregg & Rose, 1985). Flow reduction by vegetation may also facilitate larger organisms (e.g. fish; Baladrón et al., 2021), which, contrary to small-sized species, cannot escape from currents by occupying the boundary layer (of reduced velocity) on the sediment surface (Dodds & Hisaw, 1924; Brooks et al., 2005; Carlson & Lauder, 2011). Vegetation can be considered a primary shelter of flowing environments due to its relatively large, three-dimensional structure, and for the creation of near-zero flow velocities in an otherwise running habitat (Sand-Jensen, 1998).

The presence of vegetation can partially reduce the stressful conditions of running water habitats in two primary ways. First, sheltering by vegetation can reduce drag forces (Barsu et al., 2016), which limit the colonization of running habitats by large organisms that

occupy the whole water column, such as plants (Biggs, 1996). Second, vegetation reduces bed shear stress, an index of force per unit area on the bed that influences macroinvertebrates living in this zone of velocity gradient (Statzner et al., 1988), and that has been related to sediment erosion and transport (Van Rijn, 1993). Therefore, vegetation promotes the deposition of nutrient-rich fine sediment (Sand-Jensen, 1998) and supports microbial activity (Caffrey & Kemp, 1992), while a high bed shear stress can lead to fine sediment erosion and poor nutrient availability. The influence of vegetation on these physical components of the habitat gives rise to a niche with low stress in a highly stressful environment, which can increase biodiversity (Cornacchia et al., 2018).

Despite the fundamental role of vegetation sheltering in ecosystem functioning, little is known about flow adjustments downstream of a vegetated canopy in the case of live macrophytes. In particular, the distance over which vegetation provides sheltering is rarely quantified, and little is known about its variability in response to different vegetation distributions and characteristics. The sheltered area might differ for channel-spanning vegetation that is uniform in the horizontal plane (Kouwen & Unny, 1973; Nepf & Vivoni, 2000; Chen et al., 2013) compared to patches of finite width and length wherein there exists a gap between the patch and its neighbouring walls (Sand-Jensen & Vindbœk Madsen, 1992; Bouma et al., 2009; Zong & Nepf, 2012). In terms of vegetation characteristics under natural conditions, previous studies have shown that macrophyte species with contrasting morphologies create different velocity patterns downstream of their patches (Sand-Jensen & Mebus, 1996; Sand-Jensen, 1998). However, patch size, shape, or local variations in flow velocity and depth were not controlled in these field studies. This limits our ability to compare different species and generalize, or even predict their sheltering effect.

A more detailed, experimental description of the flow adjustments downstream of submerged vegetation patches comes from laboratory fluid mechanics studies, which often use plant mimics. The steady wake length (L_w) is a region where velocity and turbulence are diminished compared to the free stream (Zong & Nepf, 2012) and is strongly influenced by turbulent structures promoted within the patch. In rigid canopies, stem-scale turbulence (Liu et al., 2018) is promoted by individual stems, with a horseshoe vortex forming at the toe and von Karman vortices of vertical axis (Stoesser et al., 2006). These stem scale eddies interact within the canopy and can disappear or merge in larger structures (Chang & Constantinescu, 2015; Liu et al., 2021). Eddies may form at the patch scale: a larger horseshoe vortex around the toe of the patch (Liu et al., 2021), Kelvin-Helmoltz vortices at the canopy top (Raupach et al., 1996), and downstream von Karman vortices and a recirculation in the vertical streamwise plane (i.e., of horizontal crosswise axis; Marjoribanks et al., 2014; Liu et al., 2018). According to their size, interaction, and intensity, these eddies affect the velocities within the wake and its capacity for sheltering and sediment deposition. This was addressed in recent field experiments by Przyborowski and Łoboda (2021) and Biggs et al. (2019), who also emphasized the role of the biomass distribution along the vertical direction. This study investigates the influence of the plant species and density, and focuses on time-averaged characteristics, velocity and forces.

126 The sheltered area induced by the presence of vegetation can be determined from the
127 steady wake length. Flume studies have shown that the location and structure of vortices
128 behind a submerged patch determine the wake length (Hu et al., 2018; Liu et al., 2018) and
129 are influenced by the ratio between patch width (W) and height (h) (Liu et al. 2018; Figure 1).
130 Von Karman vortices cause lateral free-stream/wake momentum exchange, with a diffusion
131 along $W/2$ from the wake boundary to its central plane. The flow above the canopy promotes
132 crosswise, horizontal vortices causing momentum exchange from top to bottom, with a
133 diffusion along h, from canopy top to river bed. The so-called aspect ratio (W/h) might
134 markedly influence the wake length, by acting on the top to side velocities ratio, the vortices
135 formation and the length required for momentum diffusion. Considering B as the channel
136 width, the so-called patch confinement (W/B) is also expected to be influential, by modifying
137 the side velocity and also by suppressing the side velocities in aid of the top velocity alone in
138 the spanning configuration ($W/B = 1$). Particularly, the steady wake length increases with
139 patch drag, which is generally described through the nondimensional flow blockage $C_d aD$,
140 where C_d is the drag coefficient for the plants within the patch, a is frontal area per unit
141 volume, and D is patch diameter (Chen et al., 2012b). Flume studies with vegetation mimics
142 have shown that the steady wake length can range from a few to approximately 20 cm (L_w/W
143 = 0.4–1.8 for a patch width W = 10 cm) (Liu et al., 2018) and it is influenced by
144 characteristics such as density (Chen et al., 2012b; Zong & Nepf, 2012; Chang &
145 Constantinescu, 2015), flexibility (Hu et al., 2018) and patch geometry (Liu et al., 2018).
146 These are relevant characteristics that vary widely for natural aquatic vegetation: plant
147 patches occur in a range of sizes and aspect ratios (W/h) (Sand-Jensen & Madsen, 1992;
148 Schoelynck et al., 2012), morphological and mechanical properties (Puijalon et al., 2011) and
149 vegetation density (Bouma et al., 2007; Peralta et al., 2008). For example, Przyborowski et al.
150 (2019) investigated the flow downstream of two flexible aquatic plant species under natural
151 conditions and revealed a weaker effect on the flow field compared to rigid mimics.
152 However, the impact of vegetation characteristics on the steady wake length downstream of
153 real vegetation remains largely untested. Differences in wake lengths induced by real plants,
154 as opposed to artificial plants, can be expected for several reasons. For example, differences
155 may be due to material properties at the single plant scale (properties of artificial materials vs.
156 plant tissues such as stiffness or buoyancy but also heterogeneity of material arrangement
157 observed in plants) that determine their reconfiguration and to the spatial arrangement of
158 material that constitutes the patch (e.g., relatively irregular spatial patterns observed with live
159 vegetation or highly branched structures of certain macrophyte species as opposed to the
160 simplified structure of artificial patches). Finally, different patch characteristics co-vary in
161 real vegetation, as patch length, width and height (Licci et al., 2019), but likely also other
162 characteristics such as patch density, with small patches at the beginning of their growth
163 having possibly sparser density, compared to larger ones.

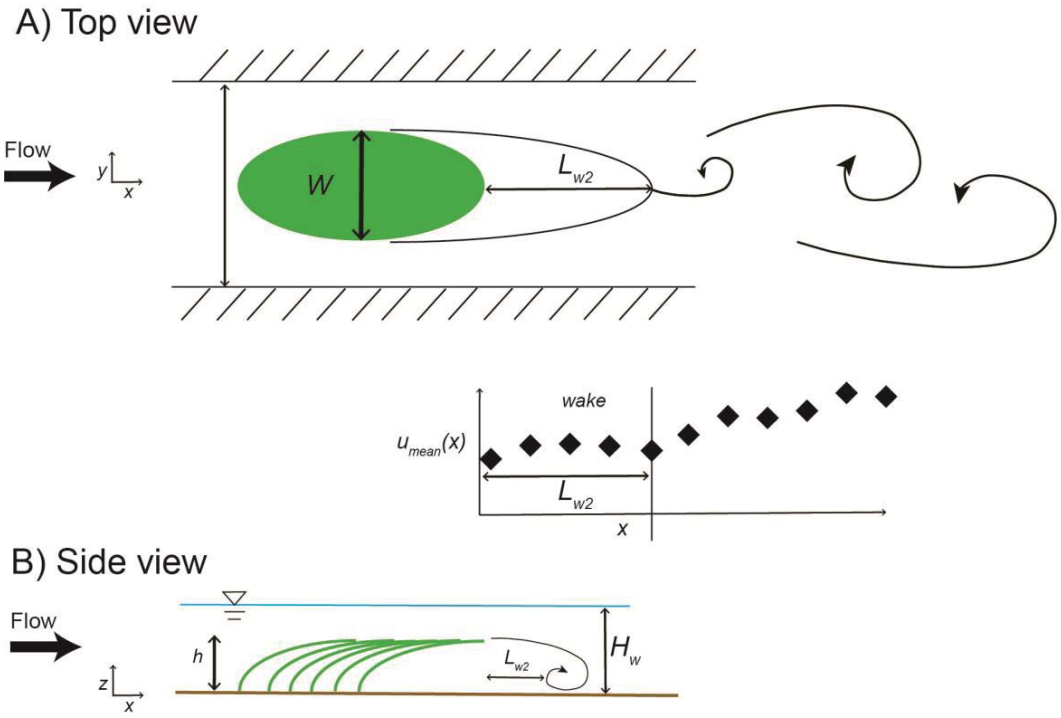

Figure 1. Schematic representation of the flow patterns behind a submerged vegetation patch with flexible stems. The development of vortical structures in the **a)** horizontal and **b)** vertical planes controls the wake length L_{w2} (distance downstream of the patch before the velocity along the patch centreline begins to increase) and depends on patch density (Zong & Nepf, 2012), as well as patch width (W) and height, defined in this study as the deflected vegetation height (h). Modified from Liu et al. (2018).

In this study, we focus on how the steady wake downstream of live macrophyte patches depends on the lateral confinement of vegetation (channel-spanning vs. finite-width patches) and plant characteristics, and on their consequences for drag force reduction behind the patches (an ecologically relevant process and an integral measure of plant adaptation to the flow; Siniscalchi and Nikora (2012)). Specifically, we test the hypothesis that, for a patch of given size and shape, different macrophyte species generate different steady wake lengths based on their morphological characteristics and biomechanical traits. Within each configuration, we vary (1) the patch aspect ratio (W/h), (2) the macrophyte species, and (3) the shoot density. Then, we assess the direct sheltering effect of these species by measuring the drag force on a plant located at different distances downstream of the patch. Although the growth of a plant would be different under natural conditions, the objective of this study is to provide a realistic quantification of the drag forces experienced by plants that attempt to establish and grow in the steady wake region.

2 Materials and Methods

2.1 Experimental channel

Experiments were performed in an outdoor flume located in the experimental garden on the campus of University Lyon 1. The channel has a straight rectangular section; is 0.8 m wide and 10 m long; and has a bed slope of 0.5%. The channel empties into a small, downstream pond, through a downstream rectangular weir with an adjustable sharp crest. The water is provided in the channel by two pipes from the combination of recirculated water from this downstream pond and of water from an upstream groundwater supply. The water temperature underwent limited daily variations during the experiments and thereby did not influence viscosity; the water temperature in the open-air channel during all measurements ranged between 15.9 and 20.7 °C and was on average 18.7 °C, as measured by the temperature sensor embedded in the Vectrino II profiler (Section 2.5). The water exits via pipes into a stilling basin that ends in a double (spanwise and vertical) convergence before entering the channel. The total discharge and weir height are adjusted to set the water depth at $H_w = 0.2$ m and the upstream mean water velocity at $U_0 = 0.05$ m s^{-1}. The flow is then turbulent (hydraulic diameter based Reynolds number $Re_{Dh} = 2.7\ 10^4$, considering a kinematic viscosity of water $\nu = 10^{-6}$ m^2 s^{-1}) and subcritical (Froude number $Fr = 0.04$). Associated stem Reynolds numbers, according to the average stem diameters of the different plants, are in the range 90–360. The estimate of the length L_{dv} required for the flow development, using the correlation (Eq. 5) proposed in Kirkgöz and Ardiçlioğlu (1997) is $L_{dv} \approx 0.3$ m. The upstream channel length $L_u = 5$ m is significantly bigger than L_{dv}, and the flow is expected to be fully developed before reaching the patch. The flume bed was composed of a mixture of sand and gravel (grain size < 4 mm) to achieve more natural conditions in terms of sediment characteristics and to facilitate parts of the experimental setup (e.g., placing the metal grid with vegetation horizontally, inserting a force transducer in the sediment). The bed sediment remained stable throughout the tests, including around the vegetation, and no scouring was observed. Although real sediment was used to better represent natural conditions, a quantification of sediment erosion/deposition patterns was not the objective of this work and was not addressed.

2.2 Study species

In contrast to previous studies, which considered rigid or flexible plant mimics, we used live vegetation to maintain realistic plant characteristics. The study species were *Callitriche platycarpa* Kütz, *Groenlandia densa* (L.) Fourr. (sampled in a drainage channel of the Rhône River, near Serrières-de-Briord, France, 45.8153° N, 5.4274° E) and *Vallisneria spiralis* L. (sampled in a cut-off channel of the Rhône, 45.3401° N, 4.7760° E). Plant shoots were attached on a perforated metal grid (0.75 m × 0.5 m length) that was directly placed in the flume bed such that the grid had the same level of the bed. Sand was used to partly bury the bottom grid and minimize any potential effects on the flow structure and on turbulence generation. A plant shoot consists of a stem and leaves, but the size of the stem and leaves (relative to each other) differs between the growth forms (Figure 2). For caulescent species (*G. densa* and *C. platycarpa*), the stem is developed with long internodes. For rosette species (*V. spiralis*), the stem is reduced and partly buried. Plants were arranged with a spacing between shoots of 3.15 ± 0.36 cm for *G. densa*, 4.40 ± 0.92 cm for *V. spiralis* at high density, and 5.89 ± 1.09 cm for *V. spiralis* at low density (variability given as the mean ± SD of $n = 3$

patches of different width). Due to the complex architecture of patches of *C. platycarpa*, entire patches corresponding to the size required in the experiments were collected and transplanted on the grid to preserve the patch structure. Therefore, the shoot density and spacing for this species were determined at the end of the experiments by counting the number of individuals. The spacing between shoots for this species was estimated to be 0.97 ± 0.20 cm.

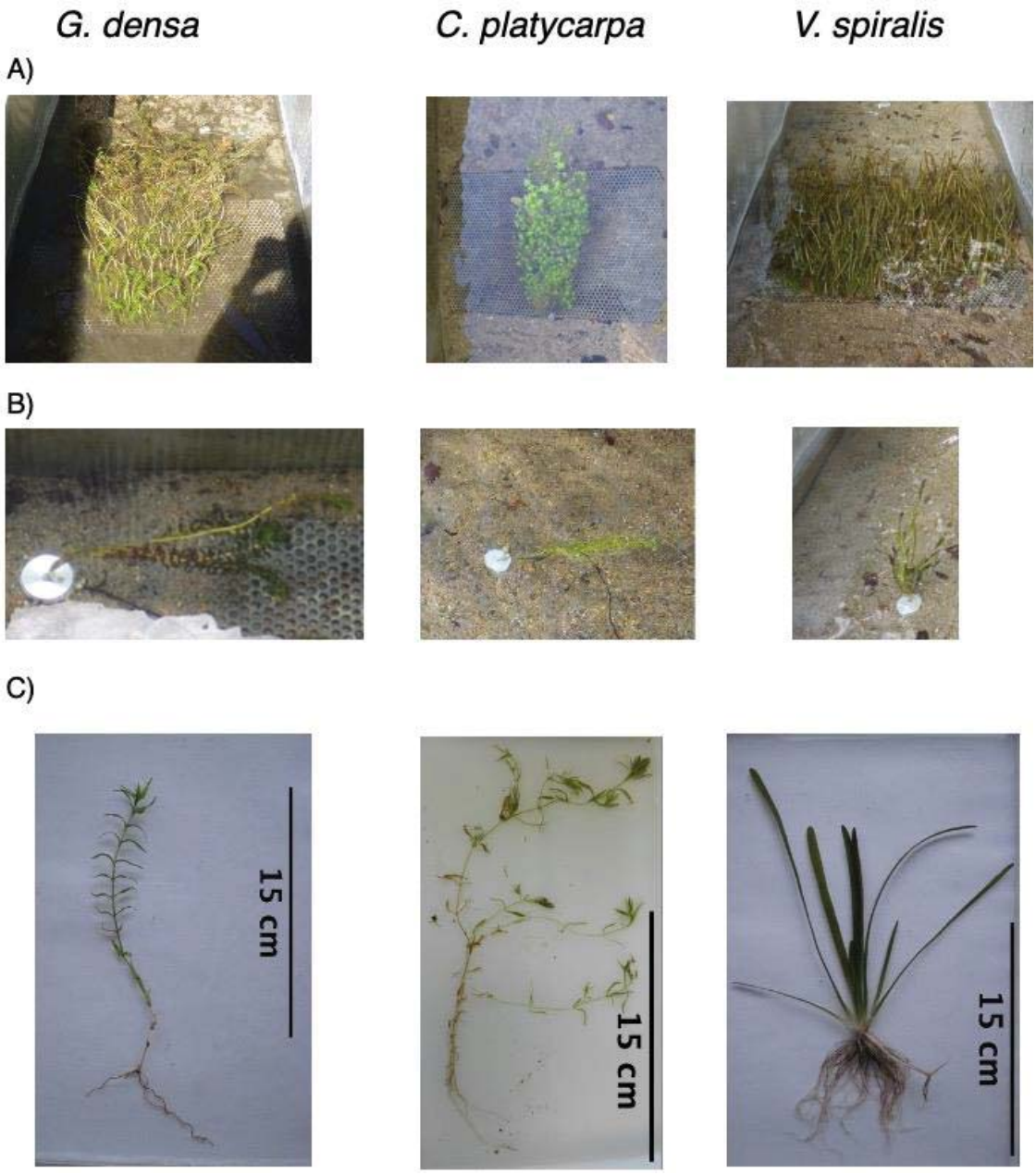

Figure 2. (A) *G. densa*, *C. platycarpa* and *V. spiralis* patches in the flume experiments; (B) single plants of each species mounted on the force transducer during the drag measurements and (C) single plants in the laboratory.

Table 1. Macrophyte species used in the flume experiments and description of their average morphological characteristics and biomechanical traits [biomass per unit surface area (kg fresh mass (FM) m^{-2}); frontal area per canopy volume (a, m^{-1}), density (n. shoots m^{-2}), Young's modulus E (MPa), second moment of area I (m^4), flexural stiffness EI (N m^2)]. Variability in patch morphological characteristics is given as the mean (± SD) of n = 3 patches of different width**s** used in the experiments. Biomechanical traits are the mean (± SD) of n = 10 individuals per species.

Species	Patch morphological characteristics			Plant biomechanical traits			Total plant surface area (m^2)
	Biomass per unit surface area (kg FM m^{-2})	Frontal area per canopy volume (a, m^{-1})	Average density (n. shoots m^{-2})	E (MPa)	I (m^4)	EI ($N\ m^2$)	
G. densa	1.31 ± 0.43	1.84 ± 0.41	1033 ± 231	42.05 ± 16.28	(5.25 ± 1.95)×10^{-13}	(2.11 ± 0.91)×10^{-5}	0.017 ± 0.002
C. platycarpa	2.14 ± 1.07	13.97 ± 6.77	11841 ± 5733	16.36 ± 0.14	(1.03 ± 0.58)×10^{-13}	(1.70 ± 1.23)×10^{-6}	0.011 ± 0.007
V. spiralis (High density)	1.57 ± 0.59	4.14 ± 1.78	567 ± 244	155.13 ± 137.41	(7.35 ± 4.82)×10^{-14}	(6.51 ± 2.56)×10^{-6}	0.014 ± 0.004
V. spiralis (Low density)	0.65 ± 0.23	2.27 ± 0.89	310 ± 221				

2.3 Measurements of morphological characteristics and biomechanical traits

The three species differ in morphology, biomechanical traits and density (Table 1). At the end of the experiment**s**, the patches were removed from the channel to measure their total fresh mass. Based on the area covered by each patch, the fresh mass was expressed in kg of biomass per unit surface area (kg fresh mass (FM) m^{-2}), as shown in Table 1. The number of individuals was used to calculate density (n. shoots per m^2) and to estimate the spacing between plant individuals ΔS. The frontal area per canopy volume was calculated as $a = d/\Delta S^2$, where d is the stem diameter (for *G. densa* and *C. platycarpa*) or leaf width (for *V. spiralis*), and ΔS is the average spacing between plant individuals in the patch (Nepf, 2012). The stem diameter and leaf width were measured in 10 individuals per species using a digital calliper and were on average 1.79 ± 0.16 mm for *G. densa*, 1.18 ± 0.14 mm for *C. platycarpa*, and 7.28 ± 1.10 mm for *V. spiralis*. The solid volume fraction occupied by the canopy elements, ϕ, was also calculated. For *G. densa* and *C. platycarpa*, with a circular stem cross-section, $\phi \approx (\pi/4)ad$. For *V. spiralis*, with strap-like linear leaves of width d and thickness b, $\phi = db/\Delta S^2$.

Biomechanical traits were measured through bending tests on 10 replicate individuals per species using a universal testing machine (Instron 5942, Canton, MA, USA). Mechanical forces act on the stems of species with a caulescent growth form, such as *G. densa* and *C.*

platycarpa, while the forces concentrate on leaves for species with a rosette growth form, such as *V. spiralis* (Hamann & Puijalon, 2013). Therefore, bending tests were performed on the basal part of the main stem of *G. densa* and *C. platycarpa* and on a single leaf of *V. spiralis*. Because we are working on flexible vegetation, the bending Young's modulus and flexural stiffness were chosen because they are relevant for the reconfiguration properties of the plants (Table 1).

Three-point bending tests were performed on leaf samples of *V. spiralis*. This test consists of a force applied at a constant rate of 10 mm min^{-1} at the midpoint of a sample placed on two supports (Silinski et al., 2018) with a support span of 60 mm. Due to the high flexibility of stems of *G. densa* and *C. playcarpa*, a three-point bending test could not be performed on these species. The samples were tested as cantilever beams using a one-fixed end bending test (Hamann & Puijalon, 2013), where each basal stem sample (5 cm in length) was clamped horizontally at its basal end while a force was applied at the midpoint of the sample by lowering a probe at a constant rate of 10 mm min^{-1}.

The following biomechanical traits were calculated: (1) the bending Young's modulus (E in MPa) quantifies the sample stiffness, and is defined as the slope of a sample's stress–strain curve in the elastic deformation region; (2) the second moment of area (I in m^4) quantifies the distribution of material around the axis of bending, accounting for the effect of the cross-sectional geometry of a structure on its bending stress. Because the stem cross section for *G. densa* and *C. platycarpa* was circular, I was calculated as $I = (\pi r^4)/4$, where r is the radius of the stem cross section (Niklas, 1992). Because the cross-sectional geometry of leaves of *V. spiralis* was triangular, I was calculated as $I = (bh^3)/36$, where b and d are the base and height of a triangle based on the sample leaf width and thickness; (3) the flexural stiffness (EI in N m^2) was calculated by multiplying E and I, and quantifies the resistance to bending (stiffness) of the stem or leaf fragment. A linear mixed model using maximum likelihood was used to test for differences in biomechanical traits across species. This model included species as the fixed effect and one random effect of individual plants (to account for non-independence between the plants sampled within the same patch). The dependent variables were Young's modulus, second moment of area and flexural stiffness.

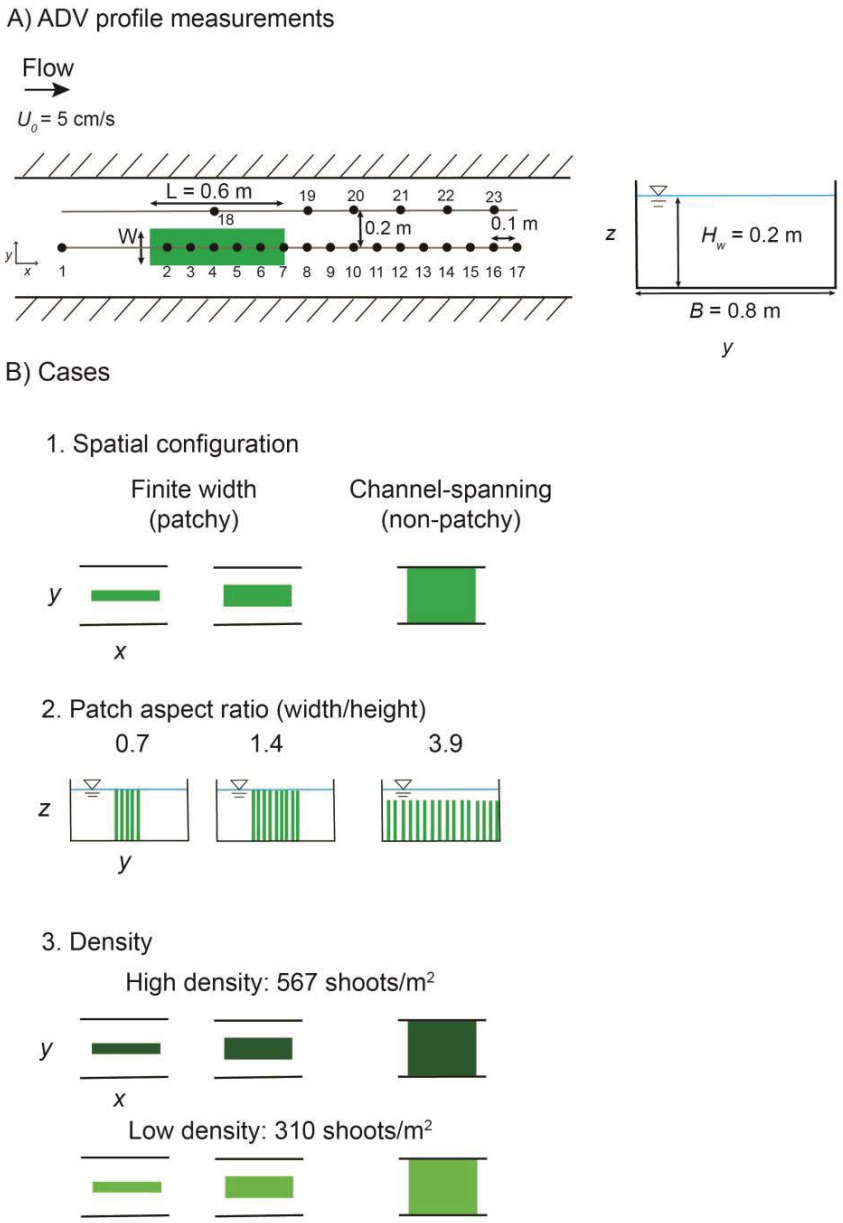

Figure 3. Schematic representation of the experimental channel and cases. **a)** Top view of the channel (with the vegetation patch shown in green) and schematic view of the channel cross-section. Numbered black dots indicate the location of flow velocity profiles measured with a Vectrino II Acoustic Doppler Velocimeter (ADV). Diagram not drawn to scale. **b)** Overview of experimental cases with varying spatial configurations, patch aspect ratios and patch densities. Note the channel-spanning case with the flow passing above the canopy (submerged) and finite-width cases where the submerged canopy can locally reach the free surface. Throughout this study, the incoming flow Reynolds number (based on the hydraulic diameter) is approximately 27000.

2.4 Patch dimensions

As shown in Figure 3b and Table 2, we compared a channel-spanning patch and two finite patches of different widths and thus the aspect ratio (*W/h*). For one species (*V. spiralis*),

we tested the effect of shoot density by removing approximately half of the shoots from each patch. Because of co-variation between different patch properties (i.e., density also changes with patch size), there is an overlap in the range of densities in the high- and low-density cases (but not in terms of biomass per unit surface area). Thus, the density effects are analysed as paired comparisons between the two cases for one given patch size. The shoot density could not be kept constant across all species primarily due to differences in biomass per shoot, which would have led to unrealistic patch characteristics. Other characteristics differ between species (e.g., biomechanical traits, morphology, biomass distribution along the stem). Thus, the choice was made to use realistic patch architecture and densities per species to recreate how they grow in natural conditions and to study density effects only within the same species.

The undeflected plant length ranged from 8–48 cm for *G. densa*, 4–45 cm for *C. platycarpa*, and 7–43 cm for *V. spiralis* (Table 2). Such a large range is expected for natural patches due to the differences in plant size between the plants in the front and rear of the patch. The patch height in this study is defined as the deflected vegetation height (h). Sideview pictures of the patches could not be taken because there was no transparent opening on the side of the outdoor flume. Using only three species also prevented us from performing quantitative analyses to compare plant deflection with the biomechanical traits. The channel blockage factor of the patch (i.e., the share of the channel cross-section occupied by the patch) was measured for all cases using underwater photographs. This parameter is relevant because the flow forced through the patch may increase with increasing channel blockage, affecting the wake length (Zong & Nepf, 2012).

2.5 Flow velocity and turbulence measurements

Flow velocity profiles were measured using an Acoustic Doppler Velocimeter (ADV), the Nortek Vectrino II profiler with a down-looking probe. The Vectrino II was used to measure the profile in 5 bins with a 3.5-cm sample length and cell size of 0.1 cm over 3 minutes at 100 Hz, to cover the depth from 0 cm from the bed to 16 cm; the top part of the flow could not be measured by the profiler due to the down-looking probe. To minimize the bed interference on the velocity measurements, only the cells located in the upper 1.5 cm were used in the calculations for the bottom part of the profile (0–3.5 cm from the bed).

Profiles were measured 1 m upstream of the vegetation patch (U_0). As shown in Figure 3a, 5 profiles were measured in the vegetation canopy (points 2–6, every 10 cm) along the patch centreline, one profile (point 7) at the downstream edge and 10 profiles downstream of the vegetation (points 8–17, every 10 cm). To minimize interference by vegetation structures within the sampling volume of the ADV probe and in the space between the probe and the sampling volume, the stems were moved aside, while the probe started at the lowest measuring point for each vertical profile within the vegetation. This process prevented the canopy from being compressed as the probe moves towards the bed (Cornacchia et al., 2019). At each ADV measurement position in the vegetation, the canopy height was measured using a tape measure. This method was preferred over point gauge measurements due to the continuous movement of the plants with the current, leading to a measurement uncertainty of

a few centimetres. Because patches of flexible macrophytes generally exhibit a gradual increase in patch height along their length (green dashed lines in Figure 4; Licci et al., 2019), both the mean and maximum patch heights are reported in Table 1. The downstream edge of the vegetation patch was identified as the end of the canopy overhanging the bed and not as the end of the rooted part.

Lateral profiles were measured along a line located 20 cm to the side of the patch centreline, and 20 cm from the flume wall. Along this line, one profile was measured halfway along the canopy length L (point 18 in Figure 3a), and 5 profiles were measured downstream of the canopy (every 20 cm; points 19–23 in Figure 3a). The velocity increase (in percent) at the lateral side of the patch was calculated as the difference between the depth-averaged velocity in profile 18 (located 20 cm to the side of the patch centreline) and the incoming depth-averaged upstream velocity U_0, divided by the upstream velocity.

Data processing was performed in MATLAB. To ensure that measurements were based on reliable data points, low-quality data points (i.e., correlation below the standard quality threshold of 70% and signal-to-noise ratio (SNR) below 15 dB) were removed during postprocessing. Data were despiked using the method described by Goring and Nikora (2002) and analysed to calculate time-averaged mean velocities. The instantaneous velocities $(u(t), v(t), w(t))$ measured in the streamwise, lateral, and vertical directions, respectively, were separated into time averages $(\overline{U}, \overline{V}, \overline{W})$, and instantaneous turbulent fluctuations $(u'(t), v'(t), w'(t))$ (e.g. as $u'(t) = u(t) - \overline{U}$, and similarly for *v* and *w*). The total turbulent kinetic energy (TKE, $m^2\ s^{-2}$) was calculated as $TKE = \frac{1}{2}\left(\overline{u'^2} + \overline{v'^2} + \overline{w'^2}\right)$.

In this study, the steady wake length is characterized in two different ways. The first definition, L_{w1}, indicates the most downstream distance (up to x/L = 2.6) where the streamwise velocity is diminished to more than half of the incoming velocity ($u < 0.5U_0$), anywhere on the vertical profile, following Boothroyd et al. (2017). The second definition, L_{w2}, is estimated to be the distance downstream of the patch before the depth-averaged velocity along the patch centreline begins to increase, as shown in Figure 1a, and denotes the distance from the patch downstream edge to the position of minimum velocity (Liu et al., 2018). This definition was chosen as it corresponds to the location where momentum injected by turbulent structures from outside accelerates the flow in the wake, marking the end of the zone sheltered by the canopy; however, defining the start of the velocity increase can be difficult, especially with a limited number of measurements. Hence, we also considered L_{w1} as an alternative, more systematic definition of the wake. In the cases where there was no clear minimum in depth-averaged velocity downstream of the patch, L_{w2} was assumed to be lower than the 0.1-m spacing between the downstream edge of the patch and the first downstream velocity profile and was therefore set to 0.05 m. This estimation of the length of the steady wake region does not account for the recovery region in which the velocity increases up to the original value upstream of the patch. This choice was made to assess the sheltering effect in a region of both reduced velocity and turbulence intensity, as opposed to the recovery region where an increase in centreline velocity and turbulence are observed (Liu et al., 2018).

2.6 Drag force measurements

Drag forces were measured at points 7–17 (Figure 3a) using a custom-made force transducer (Doerler-Mesures SAS, Vandœuvre-lès-Nancy, France) that consisted of a metal foil strain gauge force transducer (single-point load cell) that measured forces in one direction with an uncertainty of ± 0.05 N. A base with a hole fitting the size of the transducer was placed in the channel bed so that the transducer placed in the hole had its top part at the same level of the channel bed. Each plant was mounted on the transducer (after elimination of belowground parts) and fixed with plastic paraffin film (Figure 2b). Drag forces were measured for 1 minute at 100 Hz. Drag measurements in some downstream locations were taken for velocities near zero. Thus, these measurements should be interpreted with care due to interference with opposing forces due to mounting of the plant on the drag sensor. Because it is impossible to mount shoots perfectly straight upwards on the drag sensor, any deviation from perfectly vertical will cause the buoyancy of the plant itself to impose a small force on the drag sensor (Bal et al., 2011). Similar considerations held for mounting the sensor on the bed due to local irregularities and grain size. To compare between species, drag was expressed as a function of the total plant surface area (Table 1). Therefore, the total surface area was obtained for each plant at the end of the drag measurements. The individual leaves and stems were separated, scanned and measured using WinFOLIA software (Regent Instruments Inc.). The total surface area was described by the sum of all plant parts. Drag measurements were performed on a set of two replicate plants of the same species to ensure consistency (one set for *G. densa*, one set for *C. platycarpa*, one set for *V. spiralis* high-

409 density and one for *V. spiralis* low-density). The plants used for drag measurements had a
410 size comparable to the size of the individual plants of the patch (Figure 2c).

411 The drag force per unit surface area is expected to be proportional to U^2 (for rigid
412 vegetation) or $U^{(2+\chi)}$ (for flexible vegetation), where U is the approach velocity and χ is the
413 Vogel exponent (Vogel, 1984; Västilä & Järvelä, 2014; Gosselin, 2019). For very flexible
414 vegetation that reconfigures into streamlined shape, this exponent is often negative, with $\chi \sim$
415 –1, so that an approximately linear increase of drag with flow velocity (U^1) can be expected
416 as a good fit to the data (De Langre et al., 2012). Negative values of the Vogel exponent,
417 ranging between –1.2 and –0.3, were found in previous studies (Vogel, 1984; Schutten &
418 Davy, 2000; Puijalon et al., 2005; Sand-Jensen, 2008; Bal et al., 2011). Thus, a linear
419 relationship between drag and velocity is expected in this study due to the use of highly
420 flexible and isolated plants. This relationship is tested with Pearson's correlation coefficient.

421 **3 Results**

422 3.1 Between-species comparisons of biomechanical traits

423 Results showed significant differences in biomechanical traits of the investigated species
424 (Table 1) in terms of Young's modulus (ANOVA, $F_{2,6} = 6.93$, $p = 0.03$) and flexural stiffness
425 (ANOVA, $F_{2,6} = 32.47$, $p < 0.001$). The Young's modulus of *V. spiralis* was significantly
426 higher than that of *G. densa* and *C. platycarpa* (Tukey's HSD $p < 0.02$ for both pairwise
427 comparisons). *G. densa* had the stiffest stems, with a significantly higher flexural stiffness
428 than the other two species (Tukey's HSD $p < 0.001$ for all pairwise comparisons) and the
429 highest second moment of area among the species (ANOVA, $F_{2,6} = 31.53$, $p < 0.001$). *C.*
430 *platycarpa* had the highest flexibility and lowest flexural stiffness of all three species.

431 3.2 Flow patterns around the reconfigured vegetation

432 Figure 4 shows the heights of the vegetation canopy along with plots of streamwise
433 and vertical velocities for the three vegetation configurations for each species. Because real
434 plants were used, the deflected height was not controlled in the experiments. For all species
435 and all cases, the canopy exhibited reconfiguration and particularly bending of the plants.
436 Undeflected plant lengths were indeed longer than the water depth (Table 2). Plant bending
437 decreases (the patch height increases) downstream due to the sheltering effect of upstream to
438 downstream plants (Barsu et al., 2016). Despite their bending, plants were sufficiently long to
439 still reach the water surface for finite-width cases ($\max(h/H_w) = 1$). This is consistent with
440 field conditions, where most species in shallow waters grow just below or on the water
441 surface: the submergence ratio h/H_w gradually increases with increasing patch length,
442 reaching values near 1 (Licci et al., 2019). Conversely, the plants remained below the water
443 surface for channel-spanning cases ($\max(h/H_w) = 0.8$-0.9, depending on the species). The
444 channel blockage factor was similar between the two finite-width cases (Supporting
445 Information Figure S1). The small difference in blockage factors between the two cases
446 results from adjustments of the patch where an increase in width was buffered with a
447 decrease in height; we observed less bending of the plants in the narrowest patch, except for
448 *G. densa* (cf. patch height and undeflected plant length in Table 2).

449 The changes in deflected plant height and channel blockage are related to differences
450 in the velocity field. For all species, the flow velocity within the vegetation was lower than
451 that of the incoming flow. However, due to the blockage effect in the channel-spanning case,
452 the flow was deviated by the vegetation patch towards a water layer of high velocity observed
453 on top of the canopy, while the water flow within the canopy was considerably slow (less
454 than half of the incoming depth-averaged velocity). As expected, this high-velocity water
455 layer observed in the channel-spanning case disappeared in the two finite-width patch cases
456 as the canopy reached the water surface ($h/H_w = 1$), as shown in Figure 4 by the green dashed
457 line depicting the patch shape. This phenomenon leads to differences in the vertical velocities
458 observed within the patch; nearly absent in the channel-spanning case, downwards velocities
459 are observed within the finite-width patches – depicted in Figure 4 by the downward vectors
460 for $x/L < 1$, except for *C. platycarpa* – where the flux is directed towards the bed where the
461 canopy is marginally less dense. In the two finite patch cases, the velocity increased at the
462 lateral sides of the patch, characterized by the measurement along profile 18 (Figure 3a) 0.2
463 m from the centreline. This increase (Figure 6) reached on average 111% compared to the
464 incoming depth-averaged velocity (profile 1) for *G. densa*, 83% for *C. platycarpa*, and 86%
465 for *V. spiralis* in the high-density case and 82% in the low-density case. Differences between
466 spanning and non-spanning cases were also present in the wake, downstream of the patch.
467 The channel-spanning case exhibited vertical heterogeneity in the flow velocity profiles
468 downstream of the vegetation, with faster flow in the upper part of the water column and
469 attenuated flow near the bed. This is consistent with a relatively low TKE in the wake (Figure
470 5), except in the upper part corresponding to the boundary between the wake and the upper
471 free flow, where the highest values of $-\rho\,\overline{u'w'}$ Reynolds stresses were incidentally observed
472 (Supporting Information Figure S2). The wake closed rather by momentum injected in the
473 wake from the rapid flow above. In contrast, in the finite-width patch cases, the vertical
474 velocity profiles in Figure 4 did not exhibit two layers, with low streamwise velocity
475 throughout the water column. Again, this is consistent with the TKE measurements (Figure
476 5). The bleeding flow through the non-spanning canopy produced high, quite uniform, levels
477 of TKE in the second half of the canopy and the whole wake, as observed by Chang and
478 Constantinescu (2015). Relatively strong vertical velocities were observed just downstream
479 of the patch for the particular case of *V. spiralis*, which might arise from the combined effect
480 of its plant architecture and the plant bending near the bed, similar to the vertical velocities
481 appearing when an emerging cylinder is inclined from the normal direction to the bottom
482 (Kitsikoudis et al., 2017). The streamwise velocity however increased with longitudinal
483 distance from the canopy edge. The highest levels of $-\rho\,\overline{u'v'}$ Reynolds stresses were observed
484 (Supporting Information Figure S3), characterizing a momentum injected by eddies in the
485 wake from the lateral free flows, consistently with the separated shear layers observed on the
486 sides of patches of cylinders by Chang and Constantinescu (2015).

487 Figure 6 shows the evolution of the depth-averaged velocity downstream of the patch
488 in two vertical planes, in the middle of the channel (centreline profile) and 0.2 m aside
489 (lateral profiles). The overall conclusions are similar to those based on velocities along the
490 vertical profile. As expected for the non-spanning case, lateral profiles exhibited higher
491 velocities than centreline profiles due to the obstruction effect; this effect is absent in the

492 channel-spanning case, while profiles are not strictly identical. The centreline depth-averaged
493 velocity increased more rapidly to recover U_0 for the narrowest patch, which is consistent
494 with the closing of the steady wake. The influence of the patch density appears negligible on
495 the centreline profiles, but the stronger acceleration on the laterals was stronger for the denser
496 patch of *V. spiralis*, at least for the widest non-spanning patch.

497 **Table 2.** Summary of experimental cases and results. Patch length (L) is 0.60 m for all cases. The undeflected plant length was measured on a
498 sample of 10 plants per case.

Case	**Species**	**Patch width W (m)**	**Mean patch height (m) ± SD**	**Max. patch height h (m)**	**Undeflected plant length (m)**	**Patch aspect ratio (W/L)**	**Patch aspect ratio (W/h)**	**Water height H_w (m)**	**Patch density (n. shoots m^{-2})**	**Solid volume fraction (ϕ)**	**Length of steady wake L_{w1} (m)**	**Length of steady wake L_{w2} (m)**
GRO1	*G. densa*	0.15	0.12 ± 0.06	0.21	0.26 ± 0.12	0.25	0.71	0.21	1267	0.003	0.60	0.20
GRO2	*G. densa*	0.30	0.15 ± 0.05	0.21	0.21 ± 0.11	0.50	1.43	0.21	1028	0.003	> 1.0	0.40
GRO3	*G. densa*	0.75	0.11 ± 0.06	0.19	0.21 ± 0.05	1.25	3.95	0.21	804	0.002	> 1.0	0.40
CAL1	*C. platycarpa*	0.15	0.16 ± 0.05	0.22	0.21 ± 0.08	0.25	0.68	0.22	8133	0.009	0.40	0.05
CAL2	*C. platycarpa*	0.30	0.14 ± 0.05	0.23	0.24 ± 0.12	0.50	1.30	0.23	8946	0.010	0.70	0.10
CAL3	*C. platycarpa*	0.75	0.14 ± 0.05	0.20	0.25 ± 0.08	1.25	3.75	0.23	18445	0.021	> 1.0	0.70
VAL1	*V. spiralis*	0.15	0.16 ± 0.07	0.21	0.26 ± 0.10	0.25	0.71	0.22	833	0.004	0.60	0.05
VAL2	*V. spiralis*	0.30	0.16 ± 0.05	0.21	0.28 ± 0.10	0.50	1.43	0.22	511	0.003	0.70	0.10
VAL3	*V. spiralis*	0.75	0.16 ± 0.03	0.19	0.28 ± 0.09	1.25	3.95	0.22	356	0.002	> 1.0	0.10
VAL4	*V. spiralis*	0.15	0.14 ± 0.04	0.21	0.24 ± 0.09	0.25	0.71	0.22	444	0.002	0.40	0.05
VAL5	*V. spiralis*	0.30	0.15 ± 0.06	0.21	0.28 ± 0.10	0.50	1.43	0.22	278	0.001	0.60	0.10
VAL6	*V. spiralis*	0.75	0.14 ± 0.03	0.19	0.28 ± 0.09	1.25	3.95	0.22	209	0.001	0.90	0.40

499

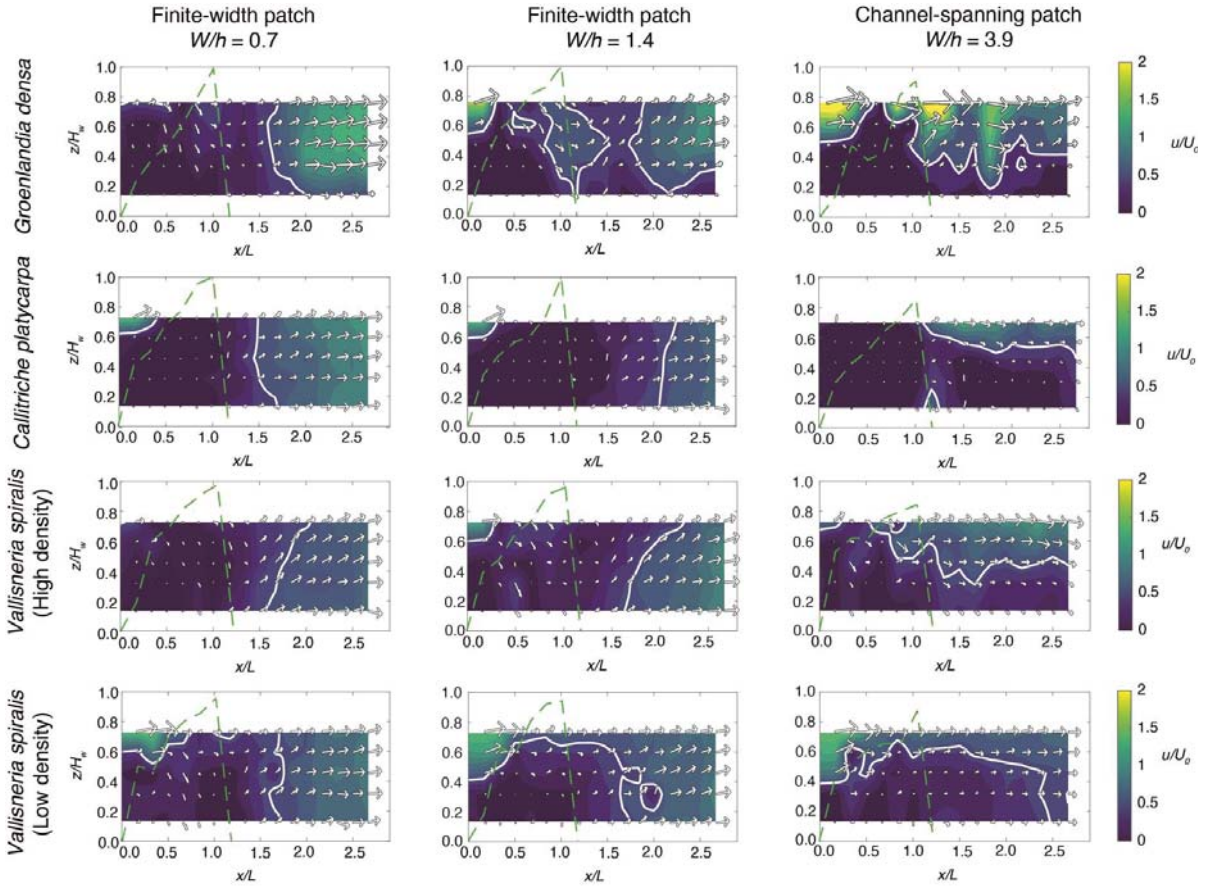

Figure 4. Resultant vector plots of streamwise and vertical velocities in the longitudinal direction. For each species, three configurations with different patch *W*/*h* ratios were considered. Green dashed lines indicate the height of the vegetation canopy. The white isoline denotes locations where the local streamwise velocity $u<0.5U_0$. The longitudinal distance (x/L) is normalized by the patch length L (60 cm for all configurations).

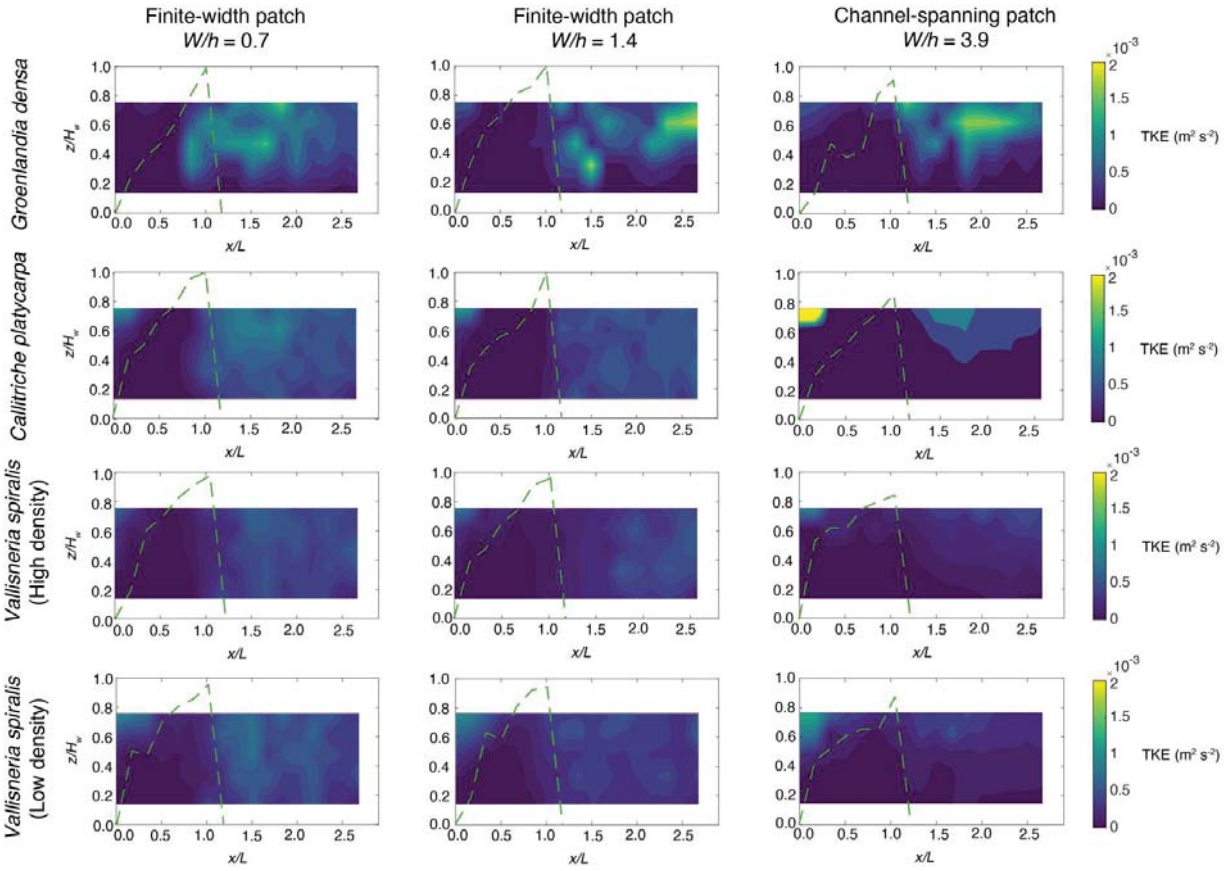

Figure 5. Colormap plots of the turbulent kinetic energy (TKE) in the central, vertical, streamwise plane. For each species, three configurations with different patch *W/h* ratios were considered. Green dashed lines indicate the height of the vegetation canopy.

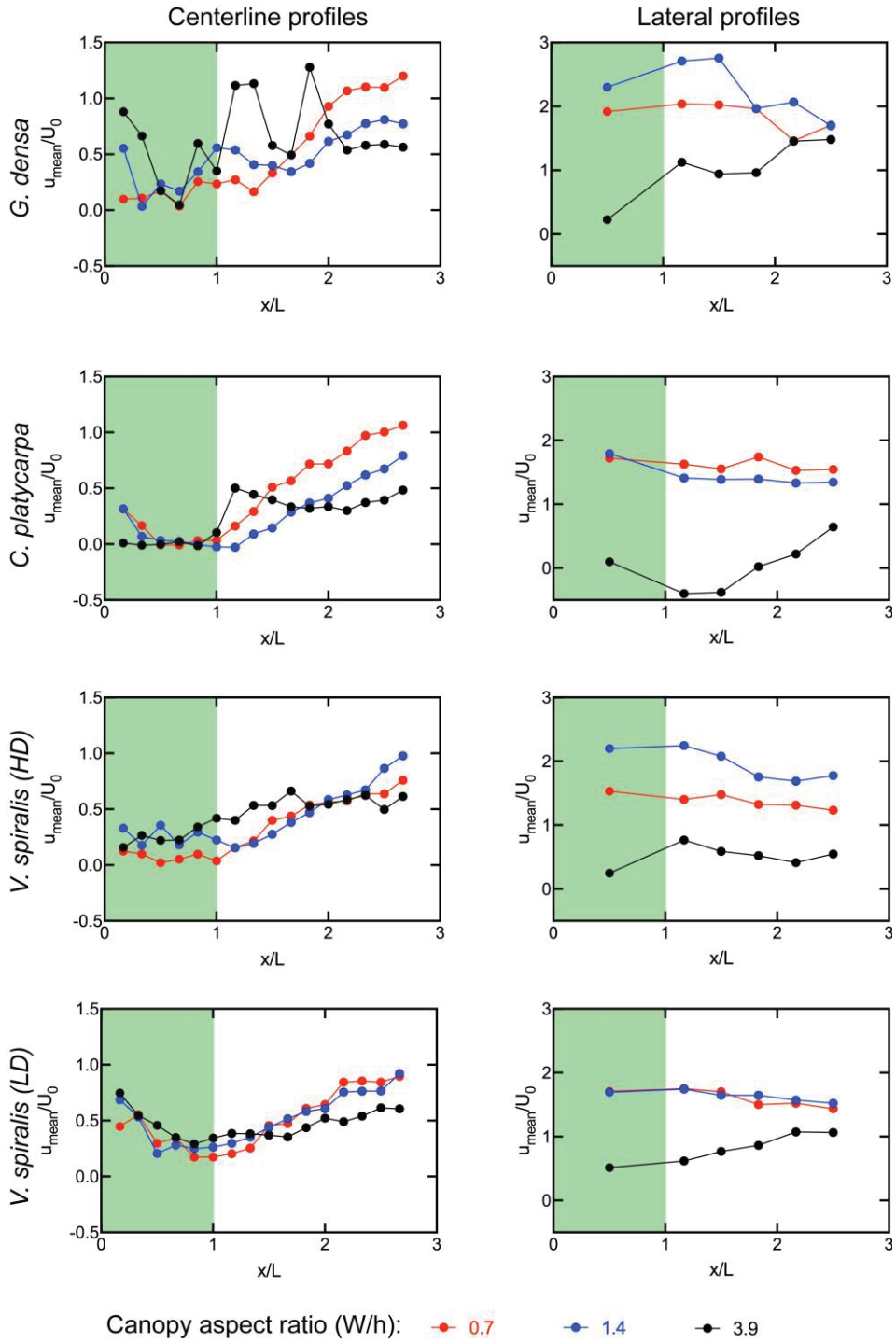

Figure 6. Longitudinal profiles of normalized depth-averaged velocity (u_{mean}/U_0) along the centreline and on the side of vegetation patches of *Groenlandia densa*, *Callitriche platycarpa* and *Vallisneria spiralis* (High and low density). The longitudinal distance (x/L) is normalized by the patch length L (60 cm for all configurations). The green shaded area indicates the location of the vegetation patch.

3.3 Steady wake length

The steady wake L_{w1} is analysed directly from Figure 4. For all species, in the channel-spanning case, L_{w1} extended to more than 2.5 patch lengths (from the patch leading edge), longer than for

the non-spanning cases, which is consistent with the blocking effect and a 2D momentum transfer from the flow above the canopy towards the bed (Figure 4). In four out of twelve cases, L_{w1} was longer than assumed a priori and was not fully resolved by the measurements (Supporting Information Figure S4). For *V. spiralis*, the wake was shorter near the bed. The rosette growth form of this species associated with a high density promoted the flow near the bed. This is similar to what was observed for such rosette plant species (*T. latifolia*; Xu and Nepf (2020)) or for isolated plants with narrow trunks near the bed, in terms of the time-averaged vertical velocity profile (Kitsikoudis et al., 2016) or wake shape (Boothroyd et al., 2017) under laboratory conditions. This rosette growth form effect, or more generally plant architecture effects, might combine with the plant bending effect near the bed, consistently with Kitsikoudis et al. (2017) where such a wake shortening near the bed was observed, jointly with the appearance of vertical velocities, for an impervious inclined cylinder. Conversely, for the three other non-spanning cases, L_{w1} was longer near the bed because the porosity was not decreased there, due to the plant structure (Figure 2; *C. platycarpa*, *G. densa*). For reference, in the profile without plants (1 m upstream of the patch), the bottom 1.9 cm of the profile had a streamwise velocity $u < 0.5U_0$.

Figure 7 shows the wake length L_{w2}, and the associated results are summarized in Table 2. Previous studies showed that the steady wake length is approximately equal to the patch width when $W < h$, or to the patch height when $W > h$ (Hu et al., 2018; Liu et al., 2018). Therefore, to make the wake lengths nondimensional, all wake lengths in Figure 7 were normalized by the canopy half-width ($W/2$) for configurations where $W/2 < h$ and by canopy height (h) for cases where $W/2 > h$. *Within* each species, measurements showed a difference between channel-spanning and finite-width patch configurations, with the dimensionless wake length $L_{w2}/min(W/2, h)$ being higher for $W/h = 3.9$, at least for two species. Conversely, within each species, the dimensionless steady wake length appears not to depend on the aspect ratio W/h for $W/h \leq 1.4$. *Between* species, in the channel-spanning patch, the dimensionless steady wake length exhibited high variability. For finite-width patch configurations, results were more homogeneous between species, except for *G. densa*. In the finite-width configurations, increasing shoot density did not significantly modify the length of the wake region for *V. spiralis* (Figures 6 and 7). However, for the channel-spanning patch, decreasing shoot density extended the steady wake length L_{w2} (Figures 6 and 7).

When comparing the two different definitions of steady wake length, relatively stable patterns emerge. According to both definitions, *G. densa* is the species that produced the longest steady wake region, and little difference in steady wake length was observed among the other three cases (Figure 6; Supporting Information Figure S4). Therefore, although the steady wake length quantified according to L_{w1} is generally longer, there is consistency across the two definitions.

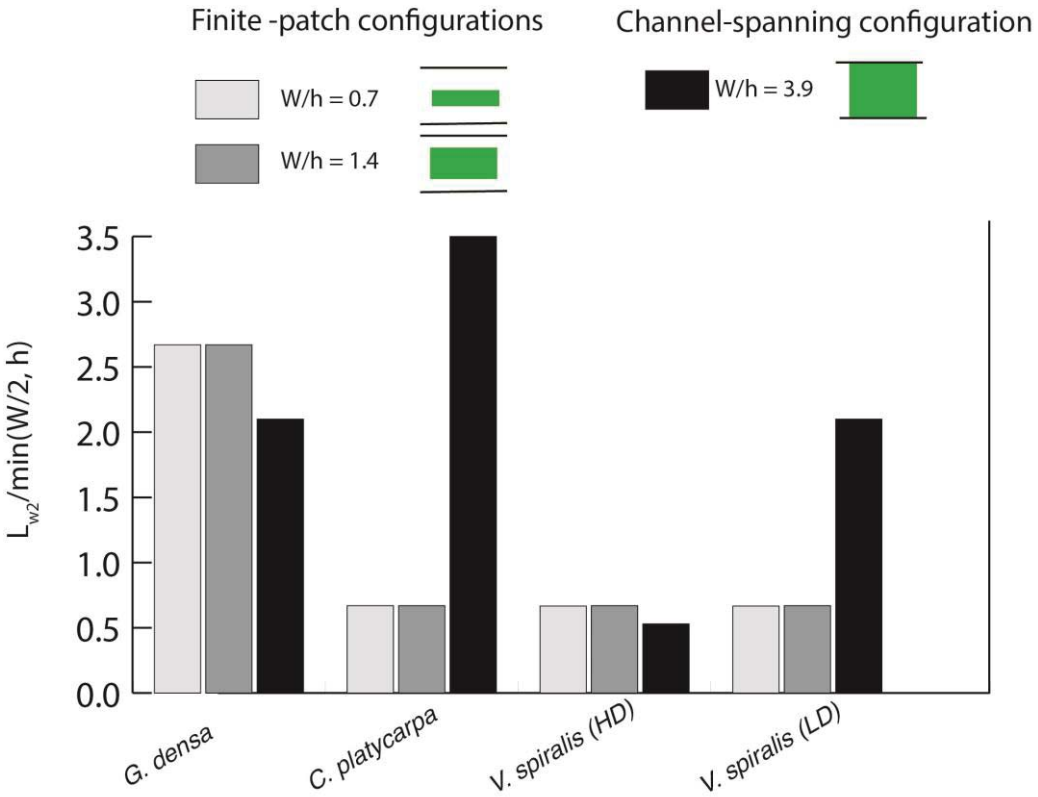

Figure 7. Dimensionless wake length (i.e., normalized by the smallest dimension between patch half-width and max. height) in the channel-spanning and two finite-patch configurations for three macrophyte species (*Groenlandia densa*, *Callitriche platycarpa* and *Vallisneria spiralis*) defined as the zone upstream of reacceleration (L_{w2}).

3.4 Drag force measurements

Figure 8 shows the measured drag force per total surface area in the wake (N m^{-2}) as a function of the corresponding normalized depth-averaged streamwise velocity (u_{mean}/U_0) at a given downstream location, taken at the same location of the drag force measurement. The 5% maximum values and variance in the measurements are summarized in more detail in the Supporting Information (Table S1). Negative drag forces at the lowest velocity are due to the weight of the plant itself imposing a small force on the drag sensor, which is related to the difficulty of mounting a shoot perfectly vertical on the drag sensor.

Measurements for two of the three species (*G. densa* and *C. platycarpa*) indicate that drag reduction is related to downstream flow modification in the case of finite-width patches but not for channel-spanning patches. We found a significant correlation between drag forces and flow velocities downstream of the vegetation for the two finite-width patches of *G. densa* (Pearsons's correlation coefficient $r = 0.59$, $p = 0.05$ for $W/h = 1.4$) and *C. platycarpa* ($r = 0.78$, $p < 0.005$ for $W/h = 0.7$; $r = 0.69$, $p < 0.05$ for $W/h = 1.4$). For high- and low-density *V. spiralis* canopies, we found a significant correlation between drag forces and downstream flow velocities for the finite-width patch configuration where $W < h$ ($r = 0.72$, $p < 0.05$ for the high-density

578 patch; r = 0.74, p < 0.01 for the low-density patch) but not for the finite-width patch where $W > h$
579 (r = 0.20, p = 0.55 for the high-density patch; r= -0.18, p = 0.6 for the low-density patch).

580 In the channel-spanning configurations (W/h = 3.9), we did not observe a significant
581 correlation between drag forces and flow velocities at a given downstream location in any of the
582 three species (r = 0.09, p = 0.79 for *G. densa*; r = 0.05, p = 0.9 for *C. platycarpa*; r = 0.33, p =
583 0.31 for *V. spiralis* high-density).

584

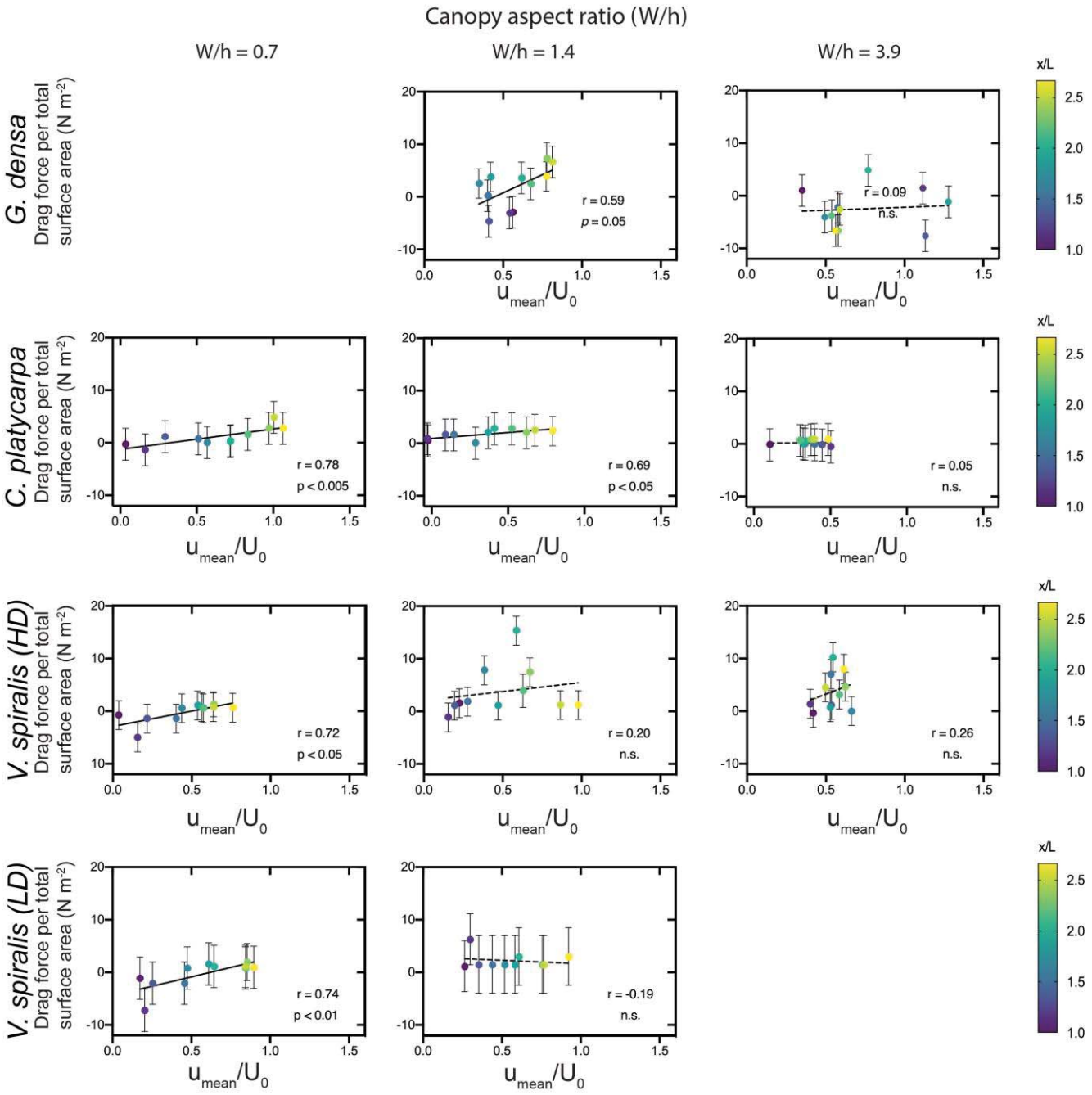

Figure 8. Relationship between normalized depth-averaged velocity (u_{mean}/U_0) and drag forces per plant total surface area (N m^{-2}) downstream of vegetation canopies. Different coloured symbols (blue–green–yellow gradient) indicate the position of the measurement point (x) normalized by the patch length L (60 cm for all configurations). Solid (dashed) lines correspond to significant (non-significant) Pearson's correlation.

4 Discussion

Vegetation canopies influence flow, sedimentation patterns and ecological processes in shallow aquatic ecosystems. While some factors that influence the sheltering effect behind vegetation patches have been investigated using vegetation mimics, this study is one of the first to compare different species of live macrophytes. We found that L_{w1} was longer behind channel-spanning patches than for finite-width patches, as expected given the increase in patch size, and extended to equal or more than 2.5 patch lengths (from the patch leading edge) for all species. For the finite-width patches, the steady wake length L_{w2} was also found to be related to the smallest dimension between the canopy half-width ($W/2$) and height (h). When normalized by the smallest of these patch dimensions, the steady wake length was comparable within each species, except for *C. platycarpa* and *V. spiralis* (low density) in the channel-spanning configuration. A second result of this study is that the velocity profiles downstream of channel-spanning real vegetation were vertically non-uniform, exhibiting a two-layer pattern that was absent behind finite-width patches, where it was compensated by a flow acceleration on the sides (Figure 9). Therefore, a shift from channel-spanning to finite-width vegetation appears to induce different flow patterns (vertical versus longitudinal variation in the flow velocity profiles), while differing patch properties (plant species and density) influence the magnitude of the process (the length of the steady wake region).

4.1 Steady wake length behind live macrophyte species: role of morphological characteristics and biomechanical traits

The results of this study indicate that patches of *G. densa* produced the longest wake regions for both L_{w1} and L_{w2} in the finite-width cases among the three species. This result might be explained by this species' more rigid stems, whose flexural stiffness was an order of magnitude higher than that of *C. platycarpa* and *V. spiralis* (Table 1). This result can also be partly attributed to morphological characteristics because patches of *G. densa* were the sparsest in terms of biomass and frontal area per canopy volume. When considering patches of finite width, *C. platycarpa* and *V. spiralis* (at both high and low densities) produced identical wake lengths. The former had a higher density and biomass per surface area, and was also the most flexible species among the studied plants; thus, a shorter wake would be expected based on previous studies (Chen et al., 2012; Zong & Nepf, 2012; Liu et al., 2021). The wake lengths were identical despite their different morphologies: *C. platycarpa* has thin, highly branched stems, while *V. spiralis* is a rosette species with strap-like leaves. Regardless, both exhibit streamlined morphologies that are adapted to running-water environments. We also observed that the finite-width patches of these two species adjusted their shape so that an increase in width was buffered with a decrease in patch height, which resulted in a small difference in channel blockage between the two finite-width cases and could explain the small difference in steady wake lengths. *Callitriche stagnalis*, a morphologically similar species, exhibits a decrease in drag coefficient with flow velocity due to reconfiguration of its shape (Siniscalchi & Nikora, 2012). Across channel-spanning cases, *C. platycarpa* had the longest wake region L_{w2} of all three species. This indicates that the trends in

steady wake length L_{w2} with increasing patch size were not consistent across species. The co-variation of patch characteristics could explain the contrasting patterns. For *C. platycarpa*, entire patches directly sampled in the field were used and their density changed with patch size: smaller patches, at the start of their growth, were sparser. The other two species showed decreasing density with patch size, which is likely an experimental artifact due to the difficulty of keeping a constant spacing between plants of variable height, shoot biomass, number of leaves and branches across patch sizes. The strong co-variation between patch characteristics, as the one observed between patch density and size for *C. platycarpa*, suggests that not all combinations of patch characteristics might occur in nature and shows the need for more studies on real vegetation and real patches.

Similar findings with regard to the importance of the minimum patch dimension (width or height) in controlling wake length for submerged vegetation were found in Hu et al. (2018), where the impact of flexible leaf mimics on the flow structure was considered. The steady wake lengths for flexible cases are longer than those in this study ($L_{xz}/min(W/2,h)$ = 11.7–18.3 for channel-spanning patches of width W = 40 cm, where L_{xz} is the distance from the patch edge to the recirculating eddy; $L_{xy}/min(W/2,h)$ = 2.4–3.8 for finite-width patches of width W = 10 cm, where L_{xy} is the distance from the patch edge to the onset of the von Karman vortices). The degree of submergence fundamentally controls wake flow dynamics (Ortiz et al., 2013; Elliott et al., 2019). Marjoribanks et al. (2019) found that the wake length downstream of flexible saltmarsh vegetation was determined by patch height rather than patch width. However, we found that both patch dimensions could determine wake length, depending on their relative size (consistent with the findings in Hu et al. 2018). We also considered fully submerged patches, while salt marsh vegetation can either emerge or be submerged depending on the tidal cycle. Finally, the plants in Marjoribanks et al. (2019) were more rigid, with a flexural stiffness that varied on the order of 10^{-5} to 10^{-3} N m^2, while in the proposed study, it varied between 10^{-5} and 10^{-6} N m^2 (Table 1).

The effect of patch shoot density on wake length was dependent on patch configuration. For finite-width patches of *V. spiralis*, wake lengths were constant despite reducing the shoot density by half. However, decreasing shoot density increased the wake length in the channel-spanning case. This effect of shoot density agrees with the findings of Chen et al. (2012) and Zong & Nepf (2012), who explained this phenomenon as greater flow through the low-density patch displaces the vortices further downstream. We caution that the effect of shoot density was tested on a single species and that the density reduction may not have been sufficient to induce significant differences in flow structure. Because we focused on patches, the density could not be too low (cf. definition of patch in Schoelynck et al. (2018)). Low shoot densities would constitute a bed of sparse plants, which is also a relevant and related question. Future research should test a broader range of patch densities to quantify the effects on downstream flow structure.

669 ### 4.2 Sheltering and drag reduction in the wake of macrophyte patches

670 A key difference in downstream flow patterns was observed in the two contrasting spatial
671 configurations of vegetation. For channel-spanning patches, near-bed flow attenuation prevailed
672 for longer distances. For finite-width patches, flow was attenuated throughout the water column,
673 possibly facilitating larger organisms, such as macrophytes. This result is supported by the
674 measurement of drag forces on plants at different distances downstream of the canopy, where
675 drag force reduction for all species was significantly related to downstream flow modifications
676 for cases where $W < h$. In these cases, only a few measurement points fell inside the sheltered
677 wake region or at a distance < 2 L_{w2}, and drag forces increased as the velocity recovers up to the
678 original value upstream of the patch. Instead, we found no significant correlation between drag
679 forces and downstream flow modifications behind channel-spanning patches. Compared to the
680 finite-width patches, most points fell within a distance that is less than two times the wake
681 length. One metre downstream of the patch, the velocity was still lower than the incoming flow
682 speed, and therefore, all points fell in a rather limited range of velocities (except in the case of *G.*
683 *densa*), which could explain the lack of correlation. While this study identified trends in drag
684 force with increasing velocity, these trends must be confirmed in future research due to the level
685 of uncertainty compared to the variation in drag forces. Therefore, we can conclude that drag
686 reduction behind patches might be significant in certain conditions and thus participate in the
687 recruitment and protection of other organisms that are possibly less tolerant to flow stress. These
688 results also confirm that vegetation patches are an important factor of flow heterogeneity in
689 rivers and contribute to habitat construction.

690 ### 4.3 Ecological implications of downstream flow patterns in field conditions

691 This study provides a basis to transfer the theory and results from fluid mechanics studies to
692 understand flow patterns around real vegetation in natural conditions. The modification of
693 hydrodynamic forces and the rates of sediment deposition vary depending on the vegetation
694 characteristics, such as species morphological characteristics and biomechanical traits or canopy
695 architecture (Sand-Jensen & Mebus, 1996; Sand-Jensen, 1998; Marjoribanks et al., 2019).
696 Regardless, this study identifies appropriate scaling parameters that relate the length over which
697 we observe flow attenuation to vegetation properties that are easily measurable in the field
698 (canopy width and height). For example, the patch width to canopy height ratio in *C. platycarpa*
699 has been reported to be 2.5 ± 1.3 in Licci et al. (2019) and 1.6 in Sand-Jensen and Pedersen
700 (2008), suggesting that the steady wake length L_{w2} will scale with the canopy height. Similarly,
701 for *G. densa*, patches can be up to a few metres in width, while plant shoots are generally 0.2 m
702 high (Cornacchia et al., 2018), which also suggests that patch wakes behind this species are
703 influenced by canopy height. Given the consistency across the two definitions of steady wake
704 length, similar considerations can be made for L_{w1}. However, care should be taken when
705 extending the results of this study into field conditions because the experimental flume was
706 narrower and more constrained than typical natural streams.

Considering the dimensional values of the steady wake length L_{w2}, this area of reduced velocity ranges from 0.05–0.15 m behind the narrowest (finite-width) patches, and is much longer (0.40–0.70 m) for the widest (channel-spanning) patches. The steady wake represents a rather large, sheltered zone in the middle of a running-water environment, which plays a significant role in habitat creation, growth and establishment of other organisms. As mentioned above, relatively small patches of 60 cm in length were used in the experiments. Patches are known to grow much longer in natural streams (e.g., Licci et al. (2019) investigated *C. platycarpa* canopies up to 2.5–3.0 m long). We can thus expect patch length to play a role in the sheltering effect, in relation to the interior adjustment length and the shear layer growth length (Rominger & Nepf, 2011). Therefore, we could also expect much longer steady wake zones for longer patches in field conditions.

In addition, the results of this study emphasize the importance of choosing realistic patch dimensions (height, width and their ratio) when building artificial patches for studies in fluid mechanics. Many additional factors create complexity when conducting experiments with real vegetation. Plant reconfiguration changes with buoyancy, which is in turn affected by photosynthesis and light**;** thus, the position of a given plant at a particular time could vary within the same day. Flexural stiffness changes with position along the stem as well as with plant age (young versus old patches). Thus, while mimics have constant and stable properties over time, live vegetation displays changes on different timescales. Finally, future research should investigate the relationship between wake length and the spacing between vegetation patches observed under natural conditions. Aquatic plants grow in regularly spaced patterns oriented parallel to the main flow direction (Cornacchia et al., 2018). The region of sheltered velocity behind a patch may have an effect on the regularity of the pattern. Gap sizes are commonly approximately 1.0 m (L. Cornacchia, personal observation), which is higher than the wake length in this study and could be due to this study using smaller patches than average. Thus, the steady wake length may determine the spacing between vegetation patches. This aspect is yet unknown and deserves further investigation. Because vegetation modifies hydrodynamic conditions and captures suspended sediment particles, a better understanding of the effects of vegetation on water flows and sediment deposition is needed to predict the future development of aquatic landscapes.

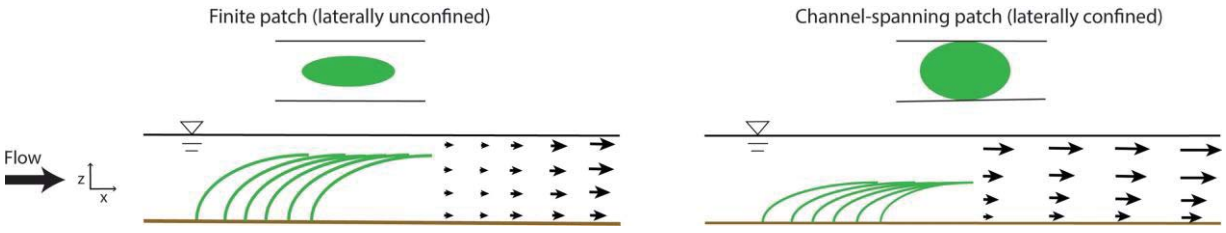

Figure 9. Schematic representation of the flow patterns downstream of finite (unconfined) and channel-spanning (confined) patches. Velocity profiles downstream of channel-spanning vegetation are vertically

non-uniform, exhibiting a two-layer pattern, which is absent for finite-width patches and is compensated by a flow acceleration on the sides.

5 Conclusions

This study investigated the flow patterns, steady wake length and the drag force on a plant behind flexible submerged vegetation patches in an outdoor flume setting. The goal of this study was to test the effect of the patch aspect ratio, species differences and shoot density on the steady wake length behind patches of live vegetation, in contrast to previous studies that used plant mimics. The primary conclusions of this study are:

1. The results of this study provide new evidence that two fundamental patch dimensions, namely canopy half-width and height, appear to be important factors that determine the steady wake length. Channel-spanning patches generally produce a longer steady wake region than finite-width patches, according to both definitions of wake (based on the $0.5U_0$ velocity limit or as the distance until flow reaccelerates). However, we also highlight that patterns of hydrodynamic sheltering behind live patches can be complex and difficult to predict based only on patch dimensions due to the co-variation between different patch characteristics (such as density and patch size), pointing to the difficulty to separate the effect of different properties when using real vegetation.
2. This study is one of the first to confirm for live vegetation that a shift from channel-spanning patches to those with finite lateral extent yields a change in hydrodynamic processes (vertical vs. longitudinal inhomogeneities in the flow velocity profiles), while differing patch properties (plant species and density) influence the magnitude of the process (the length of the steady wake region). The dimensional values of the steady wake length L_{w2} range from 0.05 to 0.70 m, which represents a rather large, sheltered zone of reduced drag and flow velocity that plays a significant role in habitat creation, recruitment and protection of other organisms.

Acknowledgments, Samples, and Data

The work was funded by the ANR-DFG 2016 project ESCaFlex (‘Experiments and simulations for the study of submerged aquatic canopies consisting of long flexible blades’, ANR-16-CE92-0020). We thank the Compagnie Nationale du Rhône (CNR) for access to field sites. This study was conducted under the aegis of the “Zone Atelier Bassin du Rhône” (ZABR, LTSER France) and the EUR H2O’Lyon (ANR-17-EURE-0018) of the Université de Lyon (UdL). We would like to thank the Editor, the Associate Editor and the anonymous reviewers for their valuable comments, which significantly improved this manuscript. We would also like to thank Heidi Nepf and Vladimir Nikora for the insightful comments and discussion on this project.

Data presented in this manuscript are available at the 4TU.Research Data repository (https://figshare.com/s/811456a0ad40aed1b55f).

References

Bal, K. D., Bouma, T. J., Buis, K., Struyf, E., Jonas, S., Backx, H., & Meire, P. (2011). Trade-off between drag reduction and light interception of macrophytes: comparing five aquatic plants with contrasting morphology. *Functional Ecology, 25*(6), 1197-1205.

Baladrón, A., Costa, M. J., Bejarano, M. D., Pinheiro, A., & Boavida, I. (2021). Can vegetation provide shelter to cyprinid species under hydropeaking? *Science of The Total Environment, 769*, 145339.

Barsu, S., Doppler, D., Jerome, J. J. S., Rivière, N., & Lance, M. (2016). Drag measurements in laterally confined 2D canopies: reconfiguration and sheltering effect. *Physics of Fluids, 28*(10), 107101.

Bertness, M. D., & Callaway, R. (1994). Positive interactions in communities. *Trends in Ecology & Evolution, 9*(5), 191-193.

Biggs, B. J. (1996). Hydraulic habitat of plants in streams. *Regulated Rivers: research & management, 12*(2-3), 131-144.

Biggs, H. J., Nikora, V., Gibbins, C., Cameron, S., Papadopoulos, K., Stewart, M., et al. (2019). Flow interactions with an aquatic macrophyte: a field study using stereoscopic particle image velocimetry. *Journal of Ecohydraulics, 4*(2), 113-130.

Boothroyd, R. J., Hardy, R. J., Warburton, J., & Marjoribanks, T. I. (2017). Modeling complex flow structures and drag around a submerged plant of varied posture. *Water Resources Research, 53*(4), 2877-2901.

Bouma, T., Friedrichs, M., Van Wesenbeeck, B., Temmerman, S., Graf, G., & Herman, P. (2009). Density-dependent linkage of scale-dependent feedbacks: A flume study on the intertidal macrophyte *Spartina anglica*. *Oikos, 118*(2), 260-268.

Bouma, T., Van Duren, L., Temmerman, S., Claverie, T., Blanco-Garcia, A., Ysebaert, T., & Herman, P. (2007). Spatial flow and sedimentation patterns within patches of epibenthic structures: Combining field, flume and modelling experiments. *Continental Shelf Research, 27*(8), 1020-1045.

Brooks, A. J., Haeusler, T., Reinfelds, I., & Williams, S. (2005). Hydraulic microhabitats and the distribution of macroinvertebrate assemblages in riffles. *Freshwater biology, 50*(2), 331-344.

Bruno, J. F., Stachowicz, J. J., & Bertness, M. D. (2003). Inclusion of facilitation into ecological theory. *Trends in Ecology & Evolution, 18*(3), 119-125.

Caffrey, J. M., & Kemp, W. M. (1992). Influence of the submersed plant, Potamogeton perfoliatus, on nitrogen cycling in estuarine sediments. *Limnology and oceanography, 37*(7), 1483-1495.

Carlson, R. L., & Lauder, G. V. (2011). Escaping the flow: boundary layer use by the darter Etheostoma tetrazonum (Percidae) during benthic station holding. *Journal of Experimental Biology, 214*(7), 1181-1193.

Chang, K., & Constantinescu, G. (2015). Numerical investigation of flow and turbulence structure through and around a circular array of rigid cylinders. *Journal of Fluid Mechanics, 776*, 161-199.

Chen, S.-C., Chan, H.-C., & Li, Y.-H. (2012a). Observations on flow and local scour around submerged flexible vegetation. *Advances in Water Resources, 43*, 28-37.

Chen, Z., Jiang, C., & Nepf, H. (2013). Flow adjustment at the leading edge of a submerged aquatic canopy. *Water Resources Research, 49*(9), 5537-5551.

824 Chen, Z., Ortiz, A., Zong, L., & Nepf, H. (2012b). The wake structure behind a porous
825 obstruction and its implications for deposition near a finite patch of emergent vegetation.
826 *Water Resources Research, 48*(9).
827 Cornacchia, L., Licci, S., Nepf, H., Folkard, A., van der Wal, D., van de Koppel, J., et al. (2019).
828 Turbulence-mediated facilitation of resource uptake in patchy stream macrophytes.
829 *Limnology and oceanography*.
830 Cornacchia, L., van de Koppel, J., van der Wal, D., Wharton, G., Puijalon, S., & Bouma, T. J.
831 (2018). Landscapes of facilitation: how self-organized patchiness of aquatic macrophytes
832 promotes diversity in streams. *Ecology, 99*(4), 832-847.
833 https://esajournals.onlinelibrary.wiley.com/doi/abs/10.1002/ecy.2177
834 Cotton, J., Wharton, G., Bass, J., Heppell, C., & Wotton, R. (2006). The effects of seasonal
835 changes to in-stream vegetation cover on patterns of flow and accumulation of sediment.
836 *Geomorphology, 77*(3), 320-334.
837 De Langre, E., Gutierrez, A., & Cossé, J. (2012). On the scaling of drag reduction by
838 reconfiguration in plants. *Comptes Rendus Mécanique, 340*(1-2), 35-40.
839 Denny, M. (1988). *Biology and the mechanics of the wave-swept environment* (Vol. 917):
840 Princeton University Press.
841 Dodds, G. S., & Hisaw, F. L. (1924). Ecological studies of aquatic Insects: Adaptations of
842 mayfly nymphs to swift streams. *Ecology, 5*(2), 137-148.
843 Elliott, S. H., Tullos, D. D., & Walter, C. (2019). Physical modeling of the feedbacks between a
844 patch of flexible Reed Canarygrass (Phalaris arundinacea), wake hydraulics, and
845 downstream deposition. *Environmental Fluid Mechanics, 19*(1), 255-277.
846 Follett, E. M., & Nepf, H. M. (2012). Sediment patterns near a model patch of reedy emergent
847 vegetation. *Geomorphology, 179*, 141-151.
848 Forman, R. T. (1995). LandMosaics: TheEcologyofLandscapesandRegions. In:
849 CambridgeUniversityPress.
850 Franklin, P., Dunbar, M., & Whitehead, P. (2008). Flow controls on lowland river macrophytes:
851 a review. *Science of the Total Environment, 400*(1), 369-378.
852 Goring, D. G., & Nikora, V. I. (2002). Despiking acoustic Doppler velocimeter data. *Journal of*
853 *Hydraulic Engineering, 128*(1), 117-126.
854 Gosselin, F. P. (2019). Mechanics of a plant in fluid flow. *Journal of Experimental Botany,*
855 *70*(14), 3533-3548.
856 Gregg, W. W., & Rose, F. L. (1985). Influences of aquatic macrophytes on invertebrate
857 community structure, guild structure, and microdistribution in streams. *Hydrobiologia,*
858 *128*(1), 45-56.
859 Gurnell, A. M. (2014). Plants as river system engineers. *Earth Surface Processes and*
860 *Landforms, 39*(1), 4-25.
861 Gurnell, A. M., & Grabowski, R. C. (2016). Vegetation–hydrogeomorphology interactions in a
862 low-energy, human-impacted river. *River Research and Applications, 32*(2), 202-215.
863 Hamann, E., & Puijalon, S. (2013). Biomechanical responses of aquatic plants to aerial
864 conditions. *Annals of botany, 112*(9), 1869-1878.
865 Haslam, S. M. (1978). *River plants: the macrophytic vegetation of watercourses*: Cambridge
866 University Press, Cambridge: 396 pp.
867 Hendriks, I. E., Sintes, T., Bouma, T. J., & Duarte, C. M. (2008). Experimental assessment and
868 modeling evaluation of the effects of the seagrass Posidonia oceanica on flow and
869 particle trapping. *Marine Ecology Progress Series, 356*, 163-173.

Hu, Z., Lei, J., Liu, C., & Nepf, H. (2018). Wake structure and sediment deposition behind models of submerged vegetation with and without flexible leaves. *Advances in Water Resources*.

Jones, C. G., Lawton, J. H., & Shachak, M. (1994). Organisms as ecosystem engineers. In *Ecosystem management* (pp. 130-147): Springer.

Kirkgöz, M. S., & Ardiçlioğlu, M. (1997). Velocity profiles of developing and developed open channel flow. *Journal of Hydraulic Engineering, 123*(12), 1099-1105.

Kitsikoudis, V., Kirca, V. O., Yagci, O., & Celik, M. F. (2017). Clear-water scour and flow field alteration around an inclined pile. *Coastal engineering, 129*, 59-73.

Kitsikoudis, V., Yagci, O., Kirca, V. O., & Kellecioglu, D. (2016). Experimental investigation of channel flow through idealized isolated tree-like vegetation. *Environmental Fluid Mechanics, 16*(6), 1283-1308.

Kouwen, N., & Unny, T. E. (1973). Flexible roughness in open channels. *Journal of the Hydraulics Division, 99*(hy5).

Licci, S., Nepf, H., Delolme, C., Marmonier, P., Bouma, T. J., & Puijalon, S. (2019). The role of patch size in ecosystem engineering capacity: a case study of aquatic vegetation. *Aquatic Sciences, 81*(3), 41.

Liu, C., Hu, Z., Lei, J., & Nepf, H. (2018). Vortex Structure and Sediment Deposition in the Wake behind a Finite Patch of Model Submerged Vegetation. *Journal of Hydraulic Engineering, 144*(2), 04017065.

Liu, M., Huai, W., & Ji, B. (2021). Characteristics of the flow structures through and around a submerged canopy patch. *Physics of Fluids, 33*(3), 035144.

Marjoribanks, T., Lague, D., Hardy, R., Boothroyd, R., Leroux, J., Mony, C., & Puijalon, S. (2019). Flexural rigidity and shoot reconfiguration determine wake length behind saltmarsh vegetation patches. *Journal of Geophysical Research: Earth Surface, 124*(8), 2176-2196.

Nepf, H. M. (2012). Flow and transport in regions with aquatic vegetation. *Annual review of fluid mechanics, 44*, 123-142.

Nepf, H. M., & Vivoni, E. (2000). Flow structure in depth-limited, vegetated flow. *Journal of Geophysical Research: Oceans, 105*(C12), 28547-28557.

Ortiz, A. C., Ashton, A., & Nepf, H. (2013). Mean and turbulent velocity fields near rigid and flexible plants and the implications for deposition. *Journal of Geophysical Research: Earth Surface, 118*(4), 2585-2599.

Peralta, G., Van Duren, L., Morris, E., & Bouma, T. (2008). Consequences of shoot density and stiffness for ecosystem engineering by benthic macrophytes in flow dominated areas: a hydrodynamic flume study. *Marine Ecology Progress Series, 368*, 103-115.

Przyborowski, Ł., Łoboda, A. M., Bialik, R. J., & Västilä, K. (2019). Flow field downstream of individual aquatic plants—Experiments in a natural river with Potamogeton crispus L. and Myriophyllum spicatum L. *Hydrological Processes, 33*(9), 1324-1337.

Puijalon, S., Bornette, G., & Sagnes, P. (2005). Adaptations to increasing hydraulic stress: morphology, hydrodynamics and fitness of two higher aquatic plant species. *Journal of Experimental Botany, 56*(412), 777-786.

Puijalon, S., Bouma, T. J., Douady, C. J., van Groenendael, J., Anten, N. P., Martel, E., & Bornette, G. (2011). Plant resistance to mechanical stress: evidence of an avoidance–tolerance trade-off. *New Phytologist, 191*(4), 1141-1149.

Rominger, J. T., & Nepf, H. M. (2011). Flow adjustment and interior flow associated with a rectangular porous obstruction.

Sand-Jensen, K. (1998). Influence of submerged macrophytes on sediment composition and near-bed flow in lowland streams. *Freshwater biology, 39*(4), 663-679.

Sand-Jensen, K. (2008). Drag forces on common plant species in temperate streams: consequences of morphology, velocity and biomass. *Hydrobiologia, 610*(1), 307-319.

Sand-Jensen, K., & Mebus, J. R. (1996). Fine-scale patterns of water velocity within macrophyte patches in streams. *Oikos, 76*(1), 169-180.

Sand-Jensen, K., & Vindbœk Madsen, T. (1992). Patch dynamics of the stream macrophyte, *Callitriche cophocarpa*. *Freshwater biology, 27*(2), 277-282.

Sand-Jensen, K. (1998). Influence of submerged macrophytes on sediment composition and near-bed flow in lowland streams. *Freshwater biology, 39*(4), 663-679.

Sand-Jensen, K., & Madsen, T. V. (1992). Patch dynamics of the stream macrophyte, Callitriche cophocarpa. *Freshwater biology, 27*(2), 277-282.

Sand-Jensen, K., & Pedersen, M. L. (2008). Streamlining of plant patches in streams. *Freshwater biology, 53*(4), 714-726.

Schoelynck, J., Creëlle, S., Buis, K., De Mulder, T., Emsens, W.-J., Hein, T., et al. (2018). What is a macrophyte patch? Patch identification in aquatic ecosystems and guidelines for consistent delineation. *Ecohydrology & Hydrobiology, 18*(1), 1-9.

Schoelynck, J., De Groote, T., Bal, K., Vandenbruwaene, W., Meire, P., & Temmerman, S. (2012). Self-organised patchiness and scale-dependent bio-geomorphic feedbacks in aquatic river vegetation. *Ecography, 35*(8), 760-768.

Schulz, M., Kozerski, H.-P., Pluntke, T., & Rinke, K. (2003). The influence of macrophytes on sedimentation and nutrient retention in the lower River Spree (Germany). *Water Research, 37*(3), 569-578.

Schutten, J., & Davy, A. (2000). Predicting the hydraulic forces on submerged macrophytes from current velocity, biomass and morphology. *Oecologia, 123*(4), 445-452.

Silinski, A., Schoutens, K., Puijalon, S., Schoelynck, J., Luyckx, D., Troch, P., et al. (2018). Coping with waves: Plasticity in tidal marsh plants as self-adapting coastal ecosystem engineers. *Limnology and Oceanography, 63*(2), 799-815.

Siniscalchi, F., & Nikora, V. I. (2012). Flow-plant interactions in open-channel flows: A comparative analysis of five freshwater plant species. *Water Resources Research, 48*(5).

Statzner, B., Gore, J. A., & Resh, V. H. (1988). Hydraulic stream ecology: observed patterns and potential applications. *Journal of the North American benthological society, 7*(4), 307-360.

Stoesser, T., Liang, C., Rodi, W., & Jirka, G. (2006). *Large eddy simulation of fully-developed turbulent flow through submerged vegetation.* Paper presented at the International conference on fluvial hydraulics, sep06-08. lisbon, portugal.

Sukhodolov, A. N., & Sukhodolova, T. A. (2009). Case study: Effect of submerged aquatic plants on turbulence structure in a lowland river. *Journal of Hydraulic Engineering, 136*(7), 434-446.

Tinoco, R. O., & Coco, G. (2016). A laboratory study on sediment resuspension within arrays of rigid cylinders. *Advances in Water Resources, 92*, 1-9.

Van Rijn, L. C. (1993). *Principles of sediment transport in rivers, estuaries and coastal seas* (Vol. 1006): Aqua publications Amsterdam.

960 Västilä, K., & Järvelä, J. (2014). Modeling the flow resistance of woody vegetation using
961 physically based properties of the foliage and stem. *Water Resources Research, 50*(1),
962 229-245.
963 Vogel, S. (1984). Drag and flexibility in sessile organisms. *American Zoologist, 24*(1), 37-44.
964 Vogel, S. (1994). *Life in moving fluids: the physical biology of flow*: Princeton University Press.
965 Wharton, G., Cotton, J. A., Wotton, R. S., Bass, J. A., Heppell, C. M., Trimmer, M., et al.
966 (2006). Macrophytes and suspension-feeding invertebrates modify flows and fine
967 sediments in the Frome and Piddle catchments, Dorset (UK). *Journal of Hydrology,*
968 *330*(1), 171-184.
969 Xu, Y., & Nepf, H. (2020). Measured and predicted turbulent kinetic energy in flow through
970 emergent vegetation with real plant morphology. *Water Resources Research, 56*(12),
971 e2020WR027892.
972 Yager, E., & Schmeeckle, M. (2013). The influence of vegetation on turbulence and bed load
973 transport. *Journal of Geophysical Research: Earth Surface, 118*(3), 1585-1601.
974 Zong, L., & Nepf, H. (2012). Vortex development behind a finite porous obstruction in a
975 channel. *Journal of Fluid Mechanics, 691*, 368-391.

976
977

Figure 1.

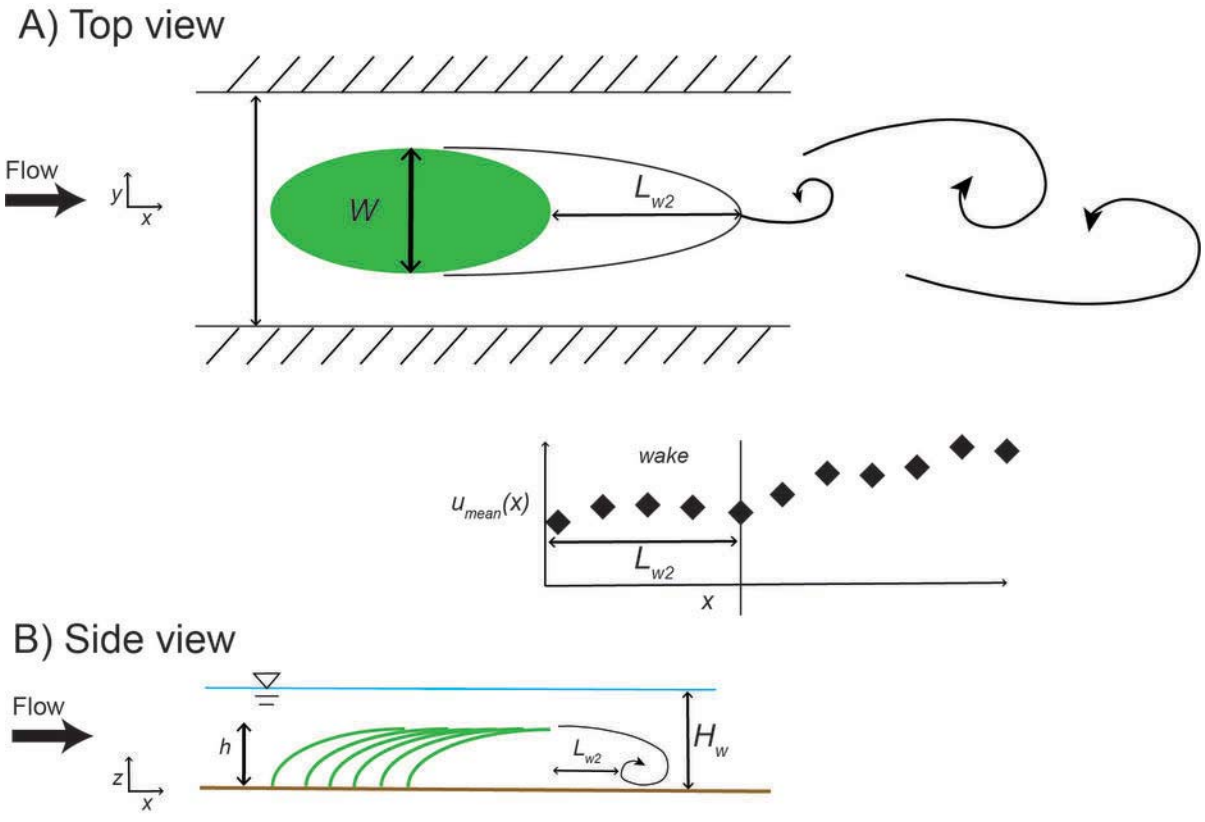
A) Top view
Flow
y
x
W
L_{w2}
wake
$u_{mean}(x)$
L_{w2}
x
B) Side view
Flow
z
x
h
L_{w2}
H_w

Figure 2.

G. densa *C. platycarpa* *V. spiralis*

A)

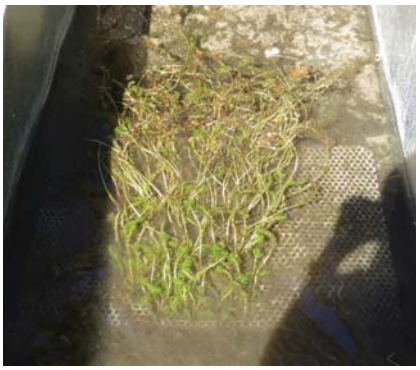

B)

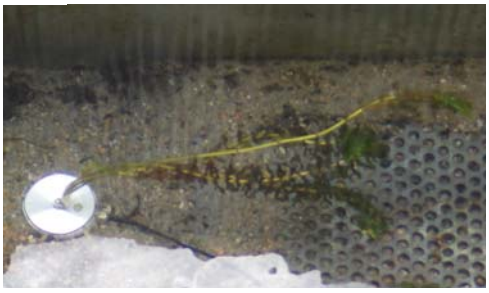

C)

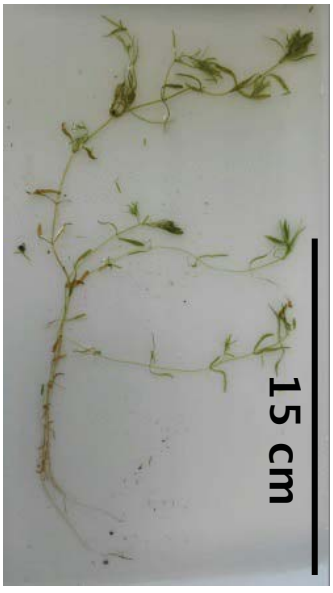

Figure 3.

A) ADV profile measurements

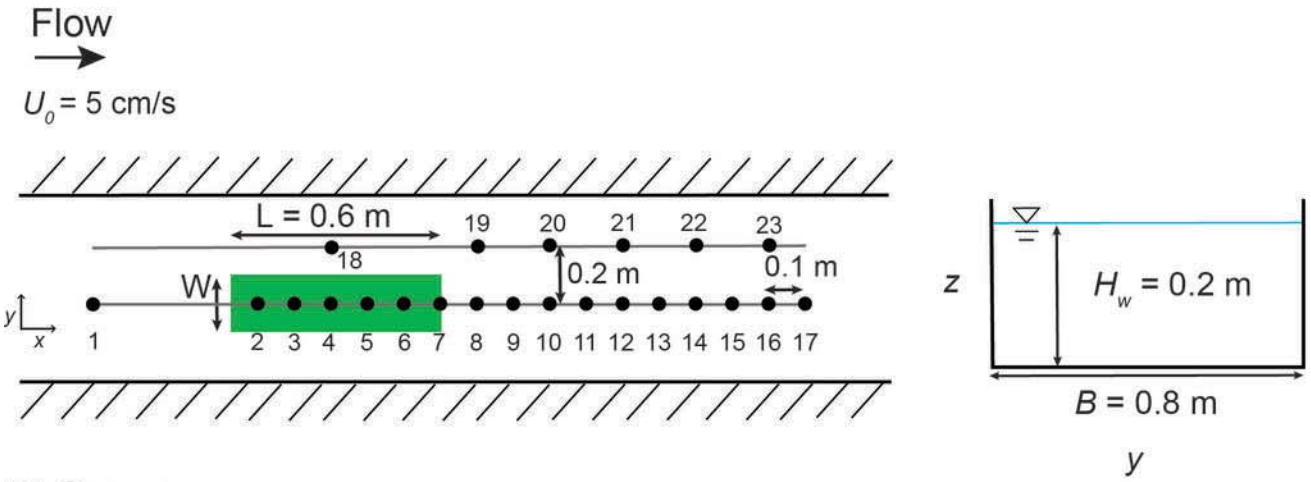

B) Cases

1. Spatial configuration

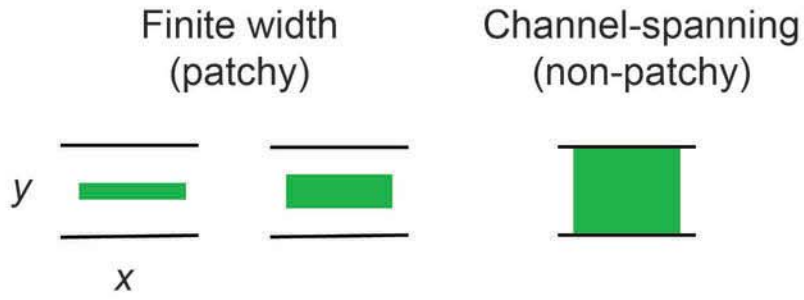

2. Patch aspect ratio (width/height)

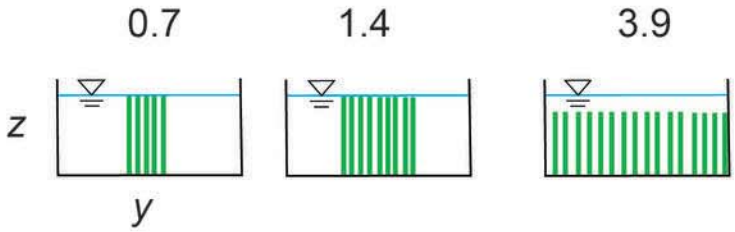

3. Density

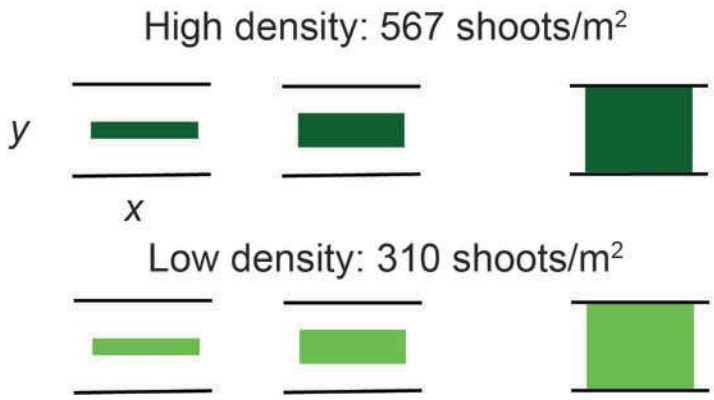

Figure 4.

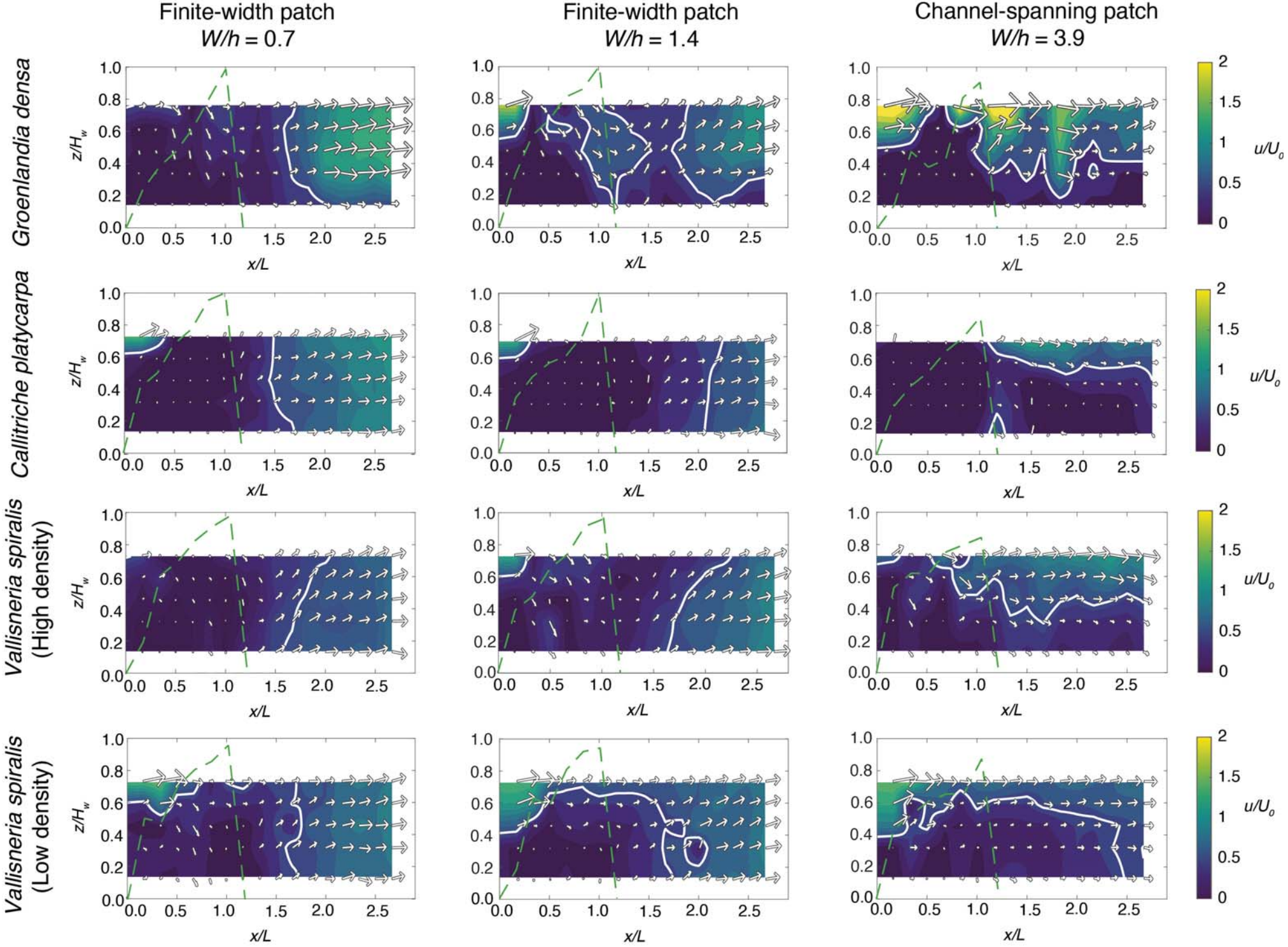
Finite-width patch
W/h = 0.7
Finite-width patch
W/h = 1.4
Channel-spanning patch
W/h = 3.9
Groenlandia densa
Callitriche platycarpa
Vallisneria spiralis
(High density)
Vallisneria spiralis
(Low density)
z/H_w
x/L
u/U_0
0.0
0.2
0.4
0.6
0.8
1.0
0.5
1.5
2.0
2.5
1
1.5
2

Figure 5.

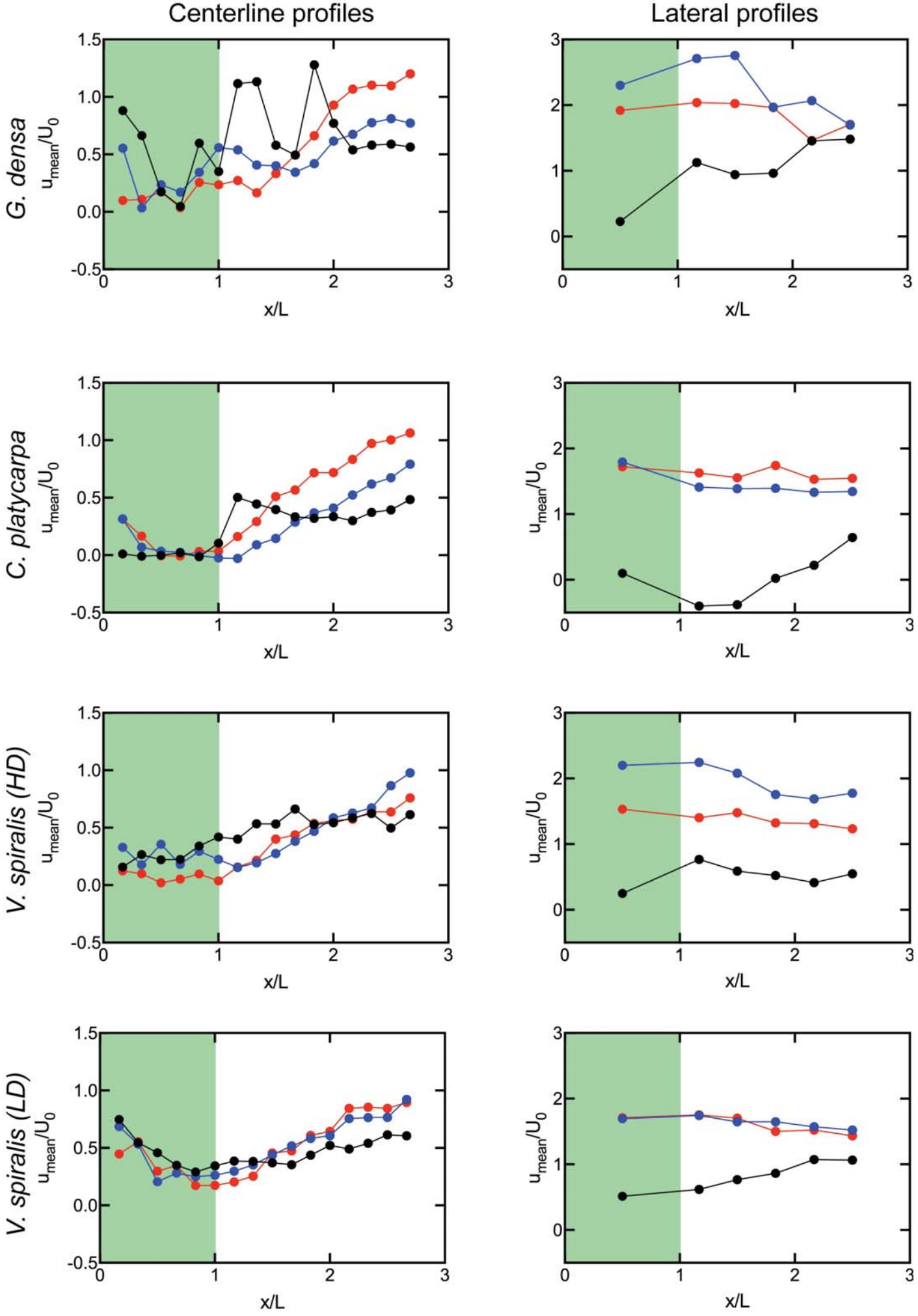
Centerline profiles
Lateral profiles
G. densa
C. platycarpa
V. spiralis (HD)
V. spiralis (LD)
u_mean/U_0
x/L
Canopy aspect ratio (W/h):
0.7
1.4
3.9

Figure 6.

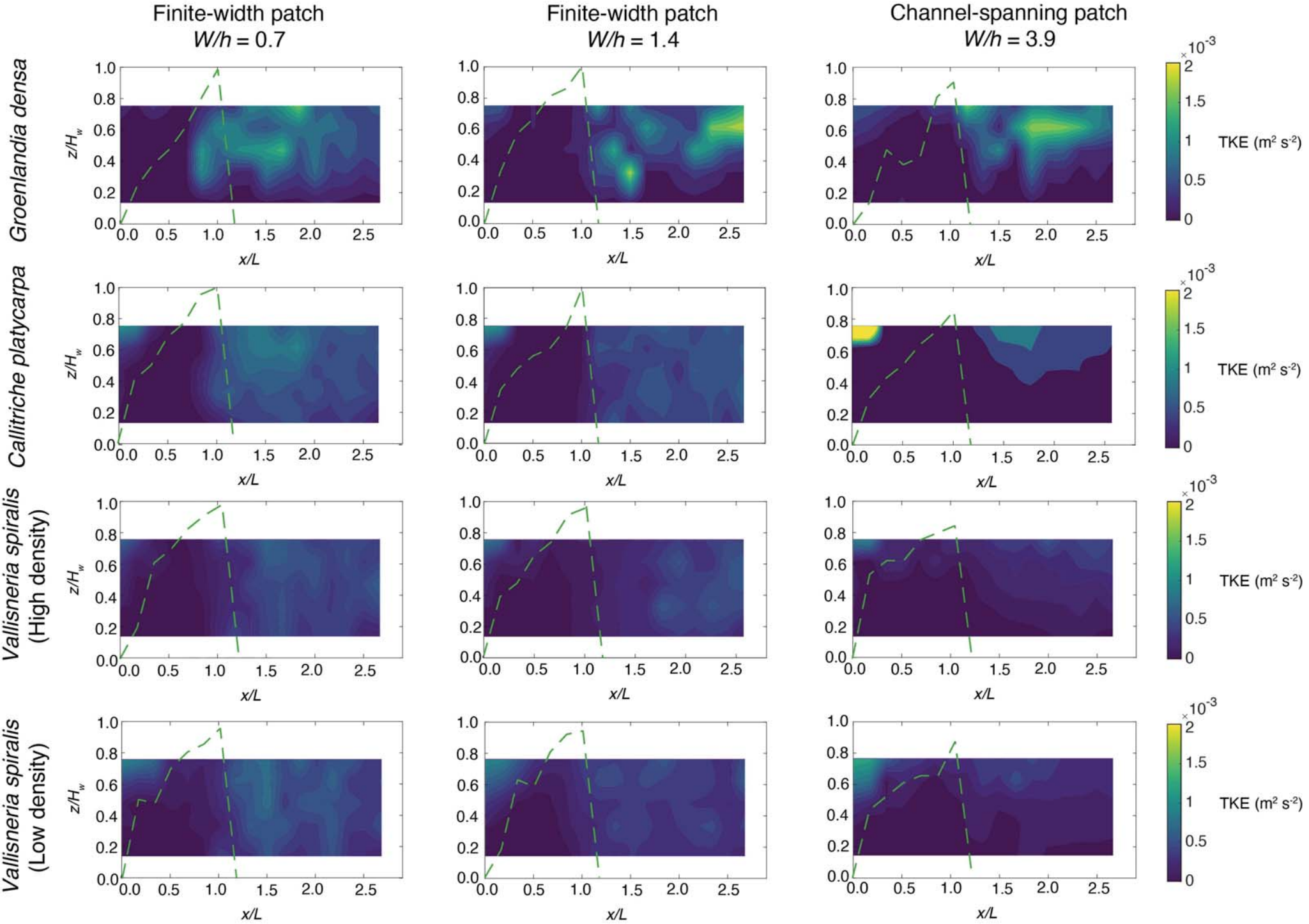
Finite-width patch
W/h = 0.7
Finite-width patch
W/h = 1.4
Channel-spanning patch
W/h = 3.9
Groenlandia densa
Callitriche platycarpa
Vallisneria spiralis
(High density)
Vallisneria spiralis
(Low density)
z/H_w
x/L
TKE (m² s⁻²)
×10⁻³

Figure 7.

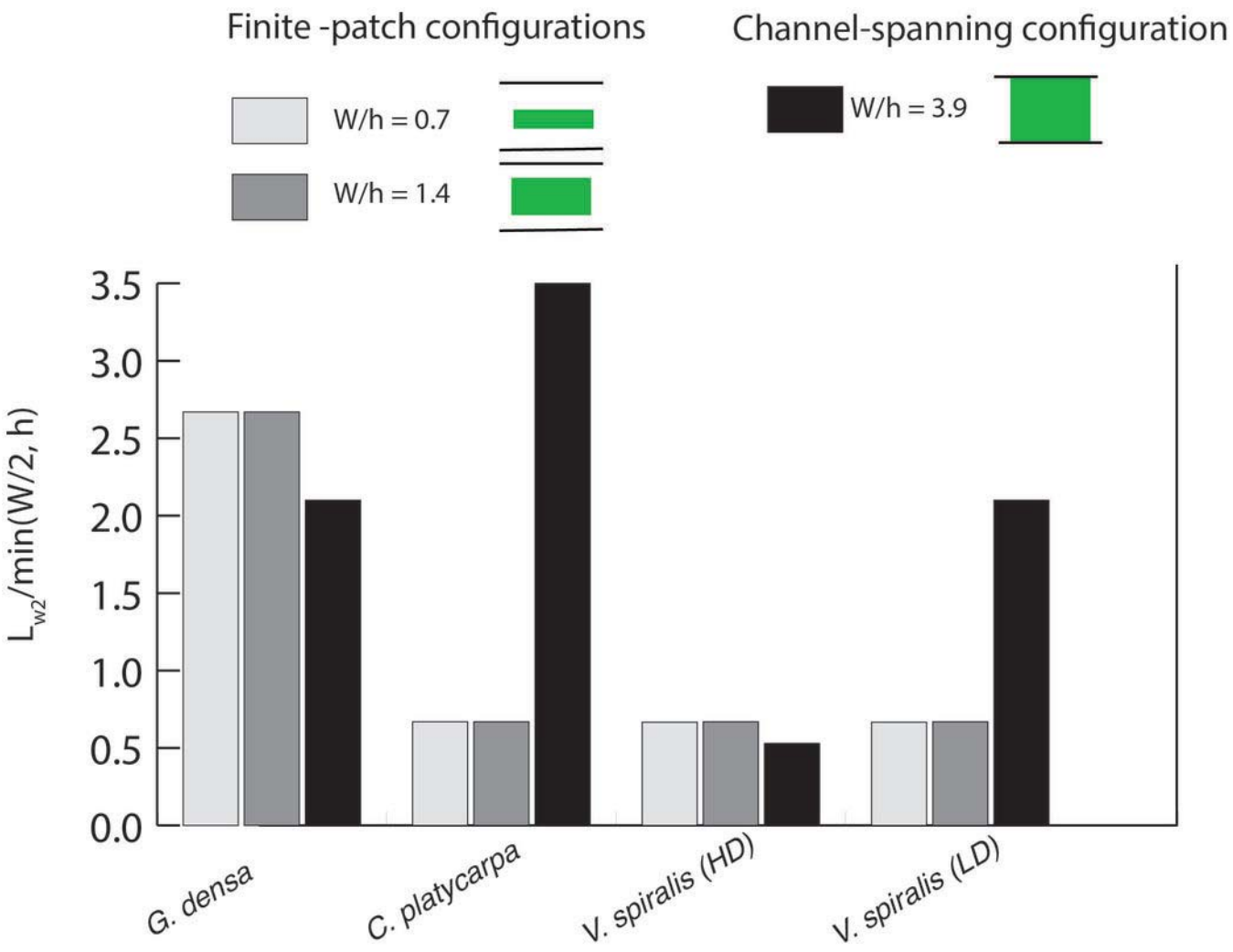
Finite -patch configurations
Channel-spanning configuration
W/h = 0.7
W/h = 1.4
W/h = 3.9
3.5
3.0
2.5
2.0
1.5
1.0
0.5
0.0
L_{w2}/min(W/2, h)
G. densa
C. platycarpa
V. spiralis (HD)
V. spiralis (LD)

Figure 8.

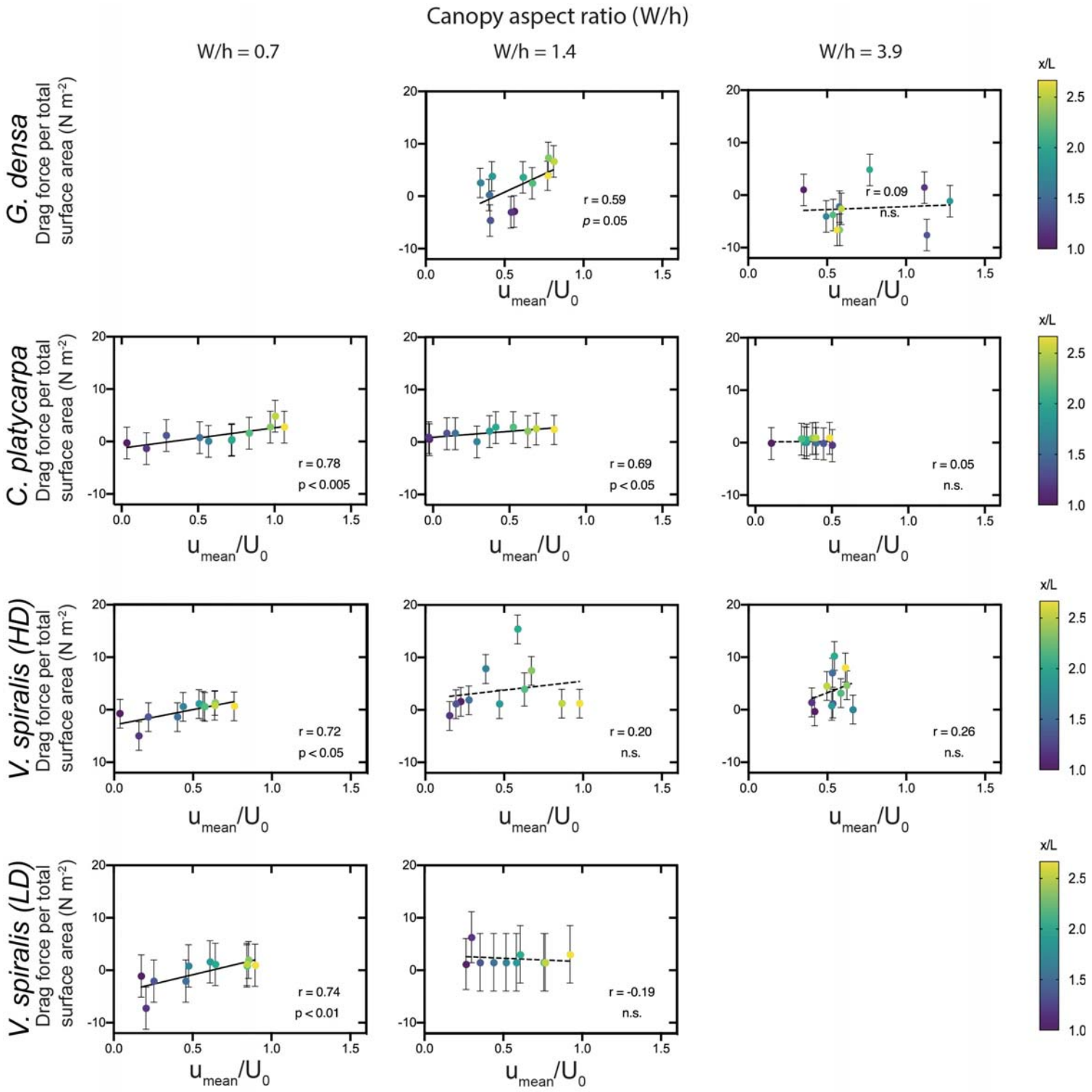
Canopy aspect ratio (W/h)
W/h = 0.7
W/h = 1.4
W/h = 3.9
G. densa
C. platycarpa
V. spiralis (HD)
V. spiralis (LD)
Drag force per total surface area (N m-2)
umean/U0
x/L
r = 0.59
p = 0.05
r = 0.09
n.s.
r = 0.78
p < 0.005
r = 0.69
p < 0.05
r = 0.05
n.s.
r = 0.72
p < 0.05
r = 0.20
n.s.
r = 0.26
n.s.
r = 0.74
p < 0.01
r = -0.19
n.s.

Figure 9.

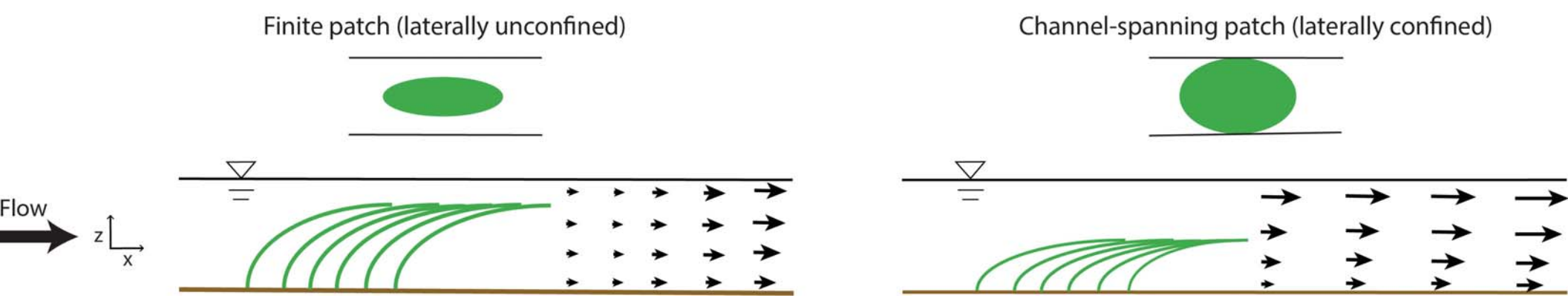
Finite patch (laterally unconfined)
Channel-spanning patch (laterally confined)
Flow
z
x